Measurement report: Molecular-level investigation of atmospheric cluster ions at the tropical high-altitude research station Chacaltaya (5240 m a.s.l.) in the Bolivian Andes

Qiaozhi Zha[1], Wei Huang[1*], Diego Aliaga[1], Otso Peräkylä[1], Liine Heikkinen[2], Alkuin Maximilian Koenig[3], Cheng Wu[4], Joonas Enroth[1], Yvette Gramlich[2], Jing Cai[1], Samara Carbone[5], Armin Hansel[6], Tuukka Petäjä[1], Markku Kulmala[1,7,8], Douglas Worsnop[1,9], Victoria Sinclair[1], Radovan Krejci[2], Marcos Andrade[10,11], Claudia Mohr[2], Federico Bianchi[1*]

[1] *Institute for Atmospheric and Earth System Research /Physics, University of Helsinki, Helsinki, Finland*

[2] *Department of Environmental Science & Bolin Centre for Climate Research, Stockholm University, Stockholm, Sweden*

[3] *Institut des Géosciences de l'Environnement, Univ Grenoble Alpes, CNRS, IRD, Grenoble INP, Grenoble, France*

[4] *Department of Chemistry & Molecular Biology, University of Gothenburg, Sweden*

[5] *Federal University of Uberlândia, Uberlândia, MG, Brazil*

[6] *Institute for Ion and Applied Physics, University of Innsbruck, Innsbruck, Austria*

[7] *Joint International Research Laboratory of Atmospheric and Earth System Sciences, Nanjing University, Nanjing, China*

[8] *Aerosol and Haze Laboratory, Beijing Advanced Innovation Center for Soft Matter Science and Engineering, Beijing University of Chemical Technology, Beijing, China*

[9] *Aerodyne Research, Inc., Billerica, MA, USA*

[10] *Laboratory for Atmospheric Physics, Institute for Physics Research, Universidad Mayor de San Andrés, La Paz, Bolivia*

[11] *epartment of Atmospheric and Oceanic Sciences, University of Maryland, College Park, MD, USA*

**Corresponding author*: Wei Huang, wei.huang@helsinki.fi and Federico Bianchi, federico.bianchi@helsinki.fi

Abstract

Air ions are the key components for a series of atmospheric physicochemical interactions, such as ion-catalyzed reactions, ion-molecule reactions, and ion-induced new particle formation. They also control atmospheric electrical properties with effects on global climate. We performed molecular-level measurements of cluster ions at the high-altitude research station Chacaltaya (CHC; 5240 m a.s.l.), located in the Bolivian Andes, from January to May 2018 using an atmospheric pressure interface time-of-flight mass spectrometer. The negative ions mainly consisted of $(H_2SO_4)_{0\text{-}3}{\cdot}HSO_4^-$, $(HNO_3)_{0\text{-}2}{\cdot}NO_3^-$, SO_5^-, $(NH_3)_{1\text{-}6}{\cdot}(H_2SO_4)_{3\text{-}7}{\cdot}HSO_4^-$, malonic acid-derived, and CHO/CHON$\cdot(HSO_4^-/NO_3^-)$ cluster ions. Their temporal variability exhibited distinct diurnal and seasonal patterns due to the changes in the corresponding neutral species' molecular properties (such as electron affinity and proton affinity) and concentrations resulting from the air masses arriving at CHC from different source regions. The positive ions were mainly composed of protonated amines and organic cluster ions, but exhibited no clear diurnal variation. H_2SO_4-NH_3 cluster ions likely contributed to the new particle formation process, particularly during wet-to-dry transition period and dry season when CHC was more impacted by air masses originating from source regions with elevated SO_2 emissions. Our study provides new insights into the chemical composition of atmospheric cluster ions and their role in new particle formation in the high-altitude mountain environment of the Bolivian Andes.

1 Introduction

Air ions regulate the electrical properties of the atmosphere by serving as carriers of electrical charges (Williams, 2009). They also play an important role in atmospheric chemistry by participating/catalyzing ion-molecule reactions and ion-induced new particle formation (NPF, Hirsikko et al., 2011). The formation of tropospheric ions is initiated through simple-structured ions, such as O^+, N_2^+, O^-, and O_2^-, mainly from radioactive decay in the soil (e.g., radon and gamma radiation), thunderstorm activity (lightning), and galactic cosmic rays (GCR). These ions can transfer their charges to other compounds, leading to the subsequent production of an assortment of ions, such as the bisulfate ion (HSO_4^-), nitrate ion (NO_3^-), hydronium ion (H_3O^+), and ammonium ion (NH_4^+; Smith and Spanel, 1995; Hirsikko et al., 2011). Depending on their sizes, air ions are usually classified into cluster ions (diameter ≤ 1.6 nm) that are charged molecules or molecular clusters, and charged particles (diameter > 1.6 nm; Hirsikko et al., 2005, 2011; Komppula et al., 2007).

Cluster ions exist almost always in the troposphere and can undergo frequent ion-molecule reactions during their lifetime (~100 seconds; Manninen et al., 2010; Hirsikko et al., 2011). Their chemical composition, in addition to the initial ionization, also depends on the concentrations of the parent neutral species (Eisele, 1986). Bianchi et al. (2017) showed that the diurnal cycle of negative organic ions followed the variations of their neutral molecules' concentrations in a boreal forest, since the higher

concentrations of neutral molecules would result in a larger probability of them being charged. Moreover, molecular properties of the neutral species, such as electron affinity (EA) and proton affinity (PA), are also important for determining cluster ion composition. Cluster ions derived from molecules with higher EA (e.g., HSO_4 and NO_3) or PA (e.g., trimethylamine (C_3H_9N) and pyridine (C_5H_5N)) tend to obtain the ambient negative or positive charge, respectively (Ferguson and Arnold, 1981; Hirsikko et al., 2011). Because of the strong EA or PA, it is almost unlikely that the ions derived from those molecules will further transfer their charges to other neutral compounds via ion-molecule reactions. Thus, these negative (HSO_4^- and NO_3^-) and positive ($C_3H_{10}N^+$ and $C_5H_6N^+$) ions are usually more abundant than other ions in the atmosphere (Eisele, 1986; Ehn et al., 2010; Bianchi et al., 2017; Frege et al., 2017). In contrast, charge transfer occurs more easily for ions derived from neutral species of lower EA or PA.

Atmospheric cluster ions can contribute to new particle formation (NPF) via ion-induced nucleation (Yu, 2010). Since the discovery of this mechanism in the first cloud chamber study in the early 1900s (Wilson, 1911), ion-induced nucleation has been known as an important source of atmospheric aerosol particles. Recently, a series of chamber studies conducted at the CLOUD (Cosmics Leaving Outdoor Droplets) facility at CERN (the European Centre for Nuclear Research) have shown that aerosol nucleation rates are substantially enhanced in the presence of some specific cluster ions, such as sulfuric acid – ammonia (H_2SO_4 – NH_3) cluster ions (Kirkby et al., 2011; Schobesberger et al., 2015), pure H_2SO_4 cluster ions (Kirkby et al., 2011), and organic cluster ions (Kirkby et al., 2016). Field measurements have also suggested the important role of atmospheric ions in ion-induced nucleation (Manninen et al., 2010; Hirsikko et al., 2011; Rose et al., 2018; Jokinen et al., 2018; Yan et al., 2018; Beck et al., 2021). Among them, the onsets of high-altitude NPF events, compared to those occurring in the lower troposphere, are often associated with more abundant cluster ions (Lee et al., 2003; Venzac et al., 2008; Boulon et al., 2010; Sellegri et al., 2019). Such increases are due to the higher GCR intensity and lower condensation sink (CS) in the high-altitude regions. As a result, potentially larger contributions of cluster ions to aerosol formation would be expected (Smith and Spanel, 1995; Hirsikko et al., 2011).

However, the molecular-level understanding of ambient cluster ions and their influence on NPF in high-altitude environments (in the troposphere) is still very limited. Two mountaintop studies in the Alps show that, depending on the air mass origins, NPF could be triggered by sulfuric acid-ammonia clusters, or nitrate (or sulfuric acid) clustering with highly oxygenated organic molecules (Bianchi et al., 2016; Frege et al., 2017). Another study in the Himalayas found that NPF was mainly driven by organic vapors of biogenic origin (Bianchi et al., 2021). Recently, frequent and intensive NPF events were observed at the high-altitude research station Chacaltaya (CHC; 16.3505° S, 68.1314° W; 5240 m a.s.l.) located in the Bolivian Andes (Rose et al., 2015a), but the exact mechanism and the role of cluster ions in aerosol nucleation process remain unclear. Therefore, a detailed investigation of cluster ions at CHC, including their

molecular composition, temporal variation (diurnal and seasonal), and source regions, is needed in order to understand their role in atmospheric processes such as NPF in the study regions.

Here we present measurements of atmospheric ions from January to May 2018 at CHC. The dataset is part of the Southern hemisphere high ALTitude Experiment on particle Nucleation And growth (SALTENA) field experiment campaign (Bianchi et al., 2022). During the study period, the sampled air masses originated from various source regions, such as the Amazon Basin to the east and the Altiplano and the Pacific Ocean to the west (Fig. 1a; Aliaga et al., 2021). Temporal evolution (diurnal and/or seasonal variations) of both negative and positive ion composition are investigated, and their potential connections with source regions and NPF are discussed. Our study thus adds important observational information on a better understanding of atmospheric ions and provides new insights into their role in high-altitude NPF in the troposphere of the Bolivian Andes.

2 Methods

2.1 Measurement site description

The high-altitude research station CHC is ~140 m below the summit of Mount Chacaltaya (5380 m a.s.l.) with an open view to the south and west (Andrade et al., 2015). The La Paz – El Alto metropolitan area (with 1.7 million inhabitants) is ~1 – 1.6 km lower (in altitude) and ~15 km south of CHC (Fig. 1b). The seasonal meteorological conditions at CHC depend on the cycle between the wet (November to March; wet-to-dry transition period in April) and dry (May to September; dry-to-wet transition period in October) seasons driven by large-scale tropical circulation (Rose et al., 2015a; Bianchi et al., 2022). This pattern also affects the source regions of air masses arriving at CHC (Aliaga et al., 2021). Additionally, due to the strong diurnal cycle of the planetary boundary layer (PBL) height and the thermally-induced winds in the mountainous terrain, CHC is often affected by polluted PBL transported from the La Paz – El Alto metropolitan area during daytime (Wiedensohler et al., 2018) whereas at night CHC is located in the residual layer or tropical free troposphere (Rose et al., 2015b; Chauvigné et al., 2019).

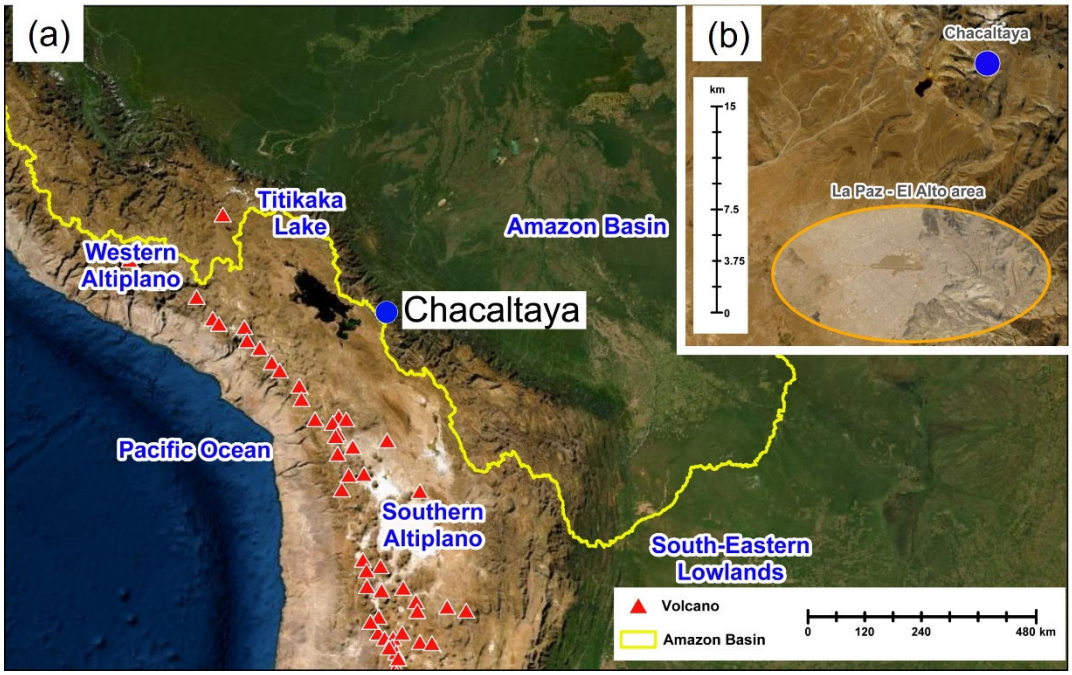

Figure 1 **(a)** True-color satellite image showing the location of CHC (blue circle) and its surrounding area. The yellow line presents the boundary of the Amazon Basin. Red triangles denote the volcanoes in this area. **(b)** A zoomed-in true-color satellite image showing the distance between CHC and the La Paz – El Alto metropolitan area (orange circle). Image sources: Esri, DigitalGlobe, GeoEye, i-cubed, USDA FSA, USGS, AEX, Getmapping, Aerogrid, IGN, IGP, swisstopo, and the GIS User Community.

2.2 Instrumentation

All the instruments involved in this study were installed in a temperature-controlled measurement room (at ~25 °C). All data are reported in local time (UTC-4).

2.2.1 Measurements of atmospheric cluster ions

The composition of cluster ions was measured by an atmospheric pressure interface time-of-flight mass spectrometer (APi-TOF, Aerodyne Research Inc. & Tofwerk AG). The APi-TOF consists of an atmospheric pressure interface (APi) module and a time-of-flight (TOF) mass spectrometer. The APi module allows the instrument to sample ions from ambient air directly. The positive or negative ions within the sampled airflow are focused and guided by two quadrupoles and an ion lens, with a gradually decreasing pressure (from atmospheric pressure to ~10^{-4} mbar), before entering the TOF mass spectrometer (~10^{-6} mbar). A more detailed description of this instrument is given in Junninen et al. (2010). In this study, ambient air was sampled through a ~1.5 m stainless steel tube with a total sample flow of 14 standard liters per minute (SLPM) to ensure laminar flow during sampling, and 0.8 SLPM of the total flow entered the APi-TOF.

During the wet season, the APi-TOF was first operated in negative mode to measure negative cluster ions (January), and then switched to positive mode to measure positive

cluster ions (February to March). During the wet-to-dry transition period (April) and dry season (May), the instrument was changed back to negative mode to investigate the potential seasonality of negative ion composition. It is important to note that, similar to Frege et al. (2017), for better characterization of the connection between cluster ions and NPF, we only included the ion data observed under the cloud-free condition in this study (to avoid influence from, e.g., lightning activity). CHC was considered to be affected by clouds when relative humidity (RH) exceeded 95 %, as suggested by a previous study at the same location (Rose et al., 2015a). From January to May 2018, the proportions of cloud-free hours to the total measurement time were 72 %, 78 %, 79 %, 98 %, and 98 %, respectively (Fig. S1).

2.2.2 Measurements of H_2SO_4 and oxidized organic molecules

Concentrations of H_2SO_4 and oxidized organic molecules (OOM) were measured using a nitrate ion (NO_3^-) based chemical ionization atmospheric pressure interface time-of-flight mass spectrometer (CI-APi-TOF, Aerodyne Research Inc. & Tofwerk AG; Jokinen et al., 2012). The instrument is a combination of the APi-TOF and a chemical ionization (CI) unit, which has been widely used to measure H_2SO_4 in the atmosphere (Jokinen et al., 2012; Bianchi et al., 2016; Zha et al., 2018). In this study, a soft X-ray source (L9490, Hamamatsu) was used to charge nitric acid (HNO_3) in a sheath flow of 20 SLPM to produce the reagent ion, NO_3^-. H_2SO_4 and OOM in the sample flow (10 SLPM) were then charged by either proton transfer or the formation of an adduct with the reagent ion during the ~200 ms residence time in the CI unit. A calibration factor of 1.5×10^{10} cm^{-3} for H_2SO_4 was determined (with sampling loss corrected) according to the approach by Kürten et al. (2012). The same calibration coefficient was adopted for determining OOM concentrations in this study, which could result in an underestimation of their concentrations due to a lower charging efficiency of OOM than H_2SO_4 by NO_3^- (Hyttinen et al., 2015).

2.2.3 Auxiliary measurements

The number concentration and size distribution of atmospheric ions and neutral particles were measured with a neutral cluster and air ion spectrometer (NAIS, Airel Ltd., Mirme and Mirme, 2013). The instrument can detect naturally charged air ions and total particles with mobility diameters from 1.4 – 50 nm and 3 – 50 nm, respectively. It is important to note that the size range of the NAIS was corrected based on a side-by-side comparison with an updated version of NAIS (designed for measurements under low pressure environments; Mirme et al., (2010)) at CHC. Thus, the size range of detection was slightly different from the traditionally reported ranges (i.e., 0.8 – 42 nm and 2 – 42 nm, respectively; Manninen et al., 2010). The details of the instrument used can be found in Rose et al. (2017).

Particle number size distributions between 10 to 500 nm were measured by a Mobility Particle Size Spectrometer (MPSS; Wiedensohler et al., 2012), and the data was used

for calculating the CS, which represents the loss rate of condensing vapors and cluster ions on pre-existing particles (Kulmala et al., 2001).

Meteorological parameters, such as temperature, RH, and global radiation, were also measured simultaneously at CHC. Detailed descriptions can be found in Bianchi et al. (2022).

2.3 Simulation of air mass origin and history

To understand the source regions and transport pathways of the air masses arriving at CHC, we used the results of air mass history analysis obtained from FLEXPART-WRF simulations described in Aliaga et al. (2021). In brief, a Lagrangian transport and dispersion model (FLEXPART-WRF; version 3.3.2; Brioude et al., 2013) was used to calculate the air mass history during the campaign period. The backward simulation was driven by the high spatial and temporal resolution meteorological output from the Weather Research and Forecasting model (WRF; version 4.0.3; Skamarock et al., 2019). In the simulation, twenty thousand particles were continuously released every hour from a 10 m deep layer (0 – 10 m a.g.l.) at CHC and traced back in the atmosphere for 96 hours. The output of the FLEXPART-WRF is the source-receptor relationship (SRR, in seconds), which is calculated for each geographical grid cell included in the simulation. The SRR value depends on the particle's residence time and the number of particles in the output grid cells. Clustering analysis was conducted by applying a series of pretreatments (e.g., log-polar grid transformation and grid cell pre-processing) and a k-means clustering algorithm (Lloyd, 1982) to the calculated SSR dataset (see Aliaga et al. (2021) for more details).

2.3.1 Major air mass pathways

Six air mass pathways (PW) representing air masses arriving at CHC were determined from the clustering analysis. They are named based on their clock positions from CHC (e.g., 03_PW indicates the pathway with its centroid located at the 3 o'clock direction (east, 90°) of CHC, Fig. 2a). Characteristics of these air mass pathways, such as source region, transport distance, and transport time, were distinct from each other (Table 1). A detailed description of the air mass pathways and their characteristics can be found in Aliaga et al. (2021).

The influence of each air mass pathway on CHC varied with time, and was estimated by its SRR percentage ($SRR[\%]_{pathway}$) as in equation (1):

$$SRR[\%]_{pathway} = \frac{SRR_{pathway}}{SRR_{total}} \times 100 \quad (1)$$

where $SRR_{pathway}$ and SRR_{total} are the residence time of a specific air mass pathway and in total (96 hours = 345600 seconds) in the simulation, respectively.

Table 1. Overview of the six air mass pathways extracted from Aliaga et al. (2021).

Pathway	Direction to CHC	Representative source region	Transport distance (km)[1] Median (25 – 75 %)	Transport time (hour) Median (25 – 75 %)
03_PW	East	Amazon Basin and Eastern/South-Eastern Lowlands	518 (413–608)	51 (45-57)
05_PW	South and Southeast	South-Eastern Lowlands and Southern Altiplano	428 (303-567)	45 (36-52)
07_PW	Southwest	The Pacific Ocean, coastal area, Western Altiplano, and La Paz – El Alto	721 (577-896)	54 (45-61)
08_PW	West	Western Altiplano and Titicaca lake, coastal area	238 (198-279)	36 (29-43)
11_PW	North and Northwest	Amazon Basin, Western Altiplano, coastal area	465 (326-563)	53 (46-59)
12_PW	North	Amazon Basin	76 (49 -95)	27 (21-33)

[1]Distance between CHC and each pathway's center point (see Fig. 2a).

2.3.2 Identification of representative periods for each air mass pathway

Air mass history analysis shows that the air sampled at CHC was typically a mixture of multiple pathways. Thus, the cluster ion composition observed during the study period was often influenced by multiple source regions concurrently. To characterize the influence of every single pathway on cluster ion composition, periods when an air mass pathway exerted its largest impact on CHC (the highest 10% of its $SRR[\%]_{pathway}$ values; Fig. 2b) during the whole study period are identified as the representative periods of the specific pathway. For instance, the representative periods of 03_PW (covering, e.g., the Amazon Basin) are more frequently seen during wet season (highest in January), whereas 08_PW (covering, e.g., Altiplano region) has most of its representative periods in dry season (highest in May). Note that $SRR[\%]_{pathway}$ of any individual pathway rarely reached 40 % due to the relatively short study period (see Fig. S2), and thus the representative periods cannot be directly identified via $SRR[\%]_{pathway}$ values. In contrast, such representative periods were determined by using a certain threshold (e.g., > 70 %) in a previous study at CHC, which was based on a more than 6-year dataset (Koenig et al., 2021).

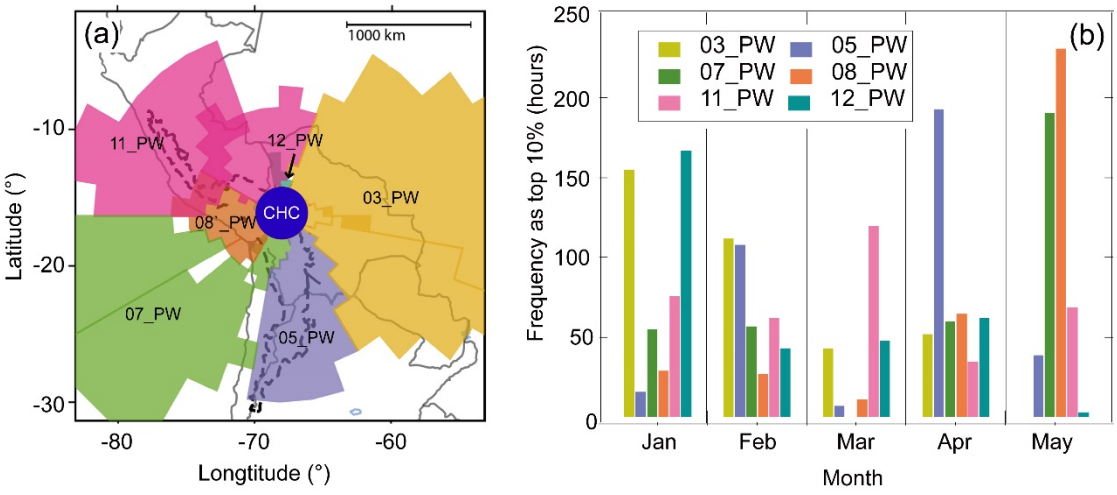

Figure 2 Influence of the six air pathways on CHC from January to May 2018. (**a**) Horizontal profile of the air mass pathways, adapted from Aliaga et al. (2021). (**b**) Frequency of the representative periods for each pathway (the highest 10% of their corresponding $SRR[\%]_{pathway}$) in different months.

3 Results and discussion

3.1 Variation in total ion count

During the study period, the total ion count (TIC) observed by APi-TOF at CHC varied between <10 and 100 counts per second (cps; Fig. 3 and Fig. S3). Similar variations in the TIC were also observed in the long-term cluster ion measurements at the high-altitude station Jungfraujoch in Switzerland (JFJ; 3454 m a.s.l.; Frege et al., 2017) and were attributed to the seasonal changes of ion precursor and sink. Like the winter–summer seasonality of the JFJ, CHC and its adjacent mountain areas are frequently covered by snow in wet season and mostly free of snow in dry season (Bianchi et al., 2022; Koenig et al., 2021). Thus, in contrast with the generally stable GCR flux (primarily controlled by the decadal scale solar cycle; Shuman et al., 2015), a reduced radioactive decay from the soil and a lower ion production rate could be expected at CHC in wet season than in dry season.

However, the TIC measured by APi-TOF was significantly higher in wet season (41 ± 23 cps, mean ± standard deviation) and the wet-to-dry transition period (56 ± 32 cps) than in dry season (14 ± 11 cps; Fig. S3). Considering the slight negative correlation (Pearson's correlation coefficient (R): –0.41; Fig. 3) between the TIC and CS (representing the loss rate of condensing vapors and cluster ions on pre-existing particles; Kulmala et al., 2001), the observed TIC fluctuation may be related (at least partially) to the varying CS (~1×10^{-4} s^{-1} in wet season to ~5×10^{-2} s^{-1} in the dry season). Moreover, the cluster ions measured by APi-TOF usually account for only a small fraction of the total atmospheric ions (Rose et al., 2018). Changes in the fraction of small ions in total atmospheric ions can potentially lead to a fluctuation in TIC (Frege

et al., 2017). This is illustrated in Figure 3 that a smaller TIC determined from APi-TOF is associated with a lower fraction of smaller ions (< 2 nm) observed by NAIS (mostly cluster ions). However, for better characterization of the influences of different ion composition on CHC and their diurnal and seasonal relative changes, we normalized the observed ion signal to the TIC for APi-TOF measurements.

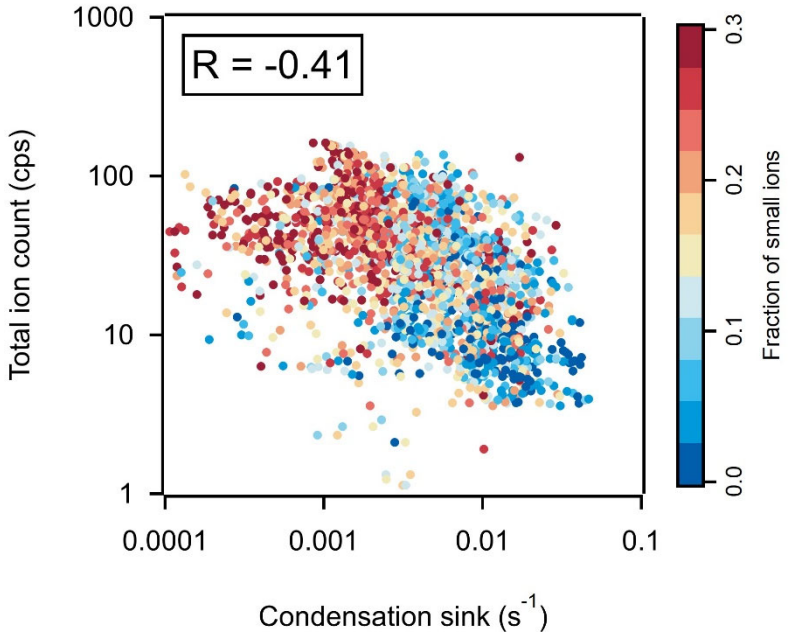

Figure 3 Correlation between the TIC measured by APi-TOF and condensation sink, colored by the fraction of small ions (defined as concentrations of ions with diameter <2 nm to the total ion concentrations) determined from NAIS data. Data are shown in the time resolution of 1 hour.

3.2 Negative ions

3.2.1 Main negative ions and their diurnal variation

A number of negative ions were consistently observed at CHC throughout the study period (i.e., in the wet, wet-to-dry transition, and dry seasons). Based on the chemical composition of the observed negative ions, we classified them into eight groups as follows: sulfuric acid ($(H_2SO_4)_{0\text{-}3}{\cdot}HSO_4^-$), nitric acid ($(HNO_3)_{0\text{-}2}{\cdot}NO_3^-$), SO_5^-, sulfuric acid-ammonia ($(NH_3)_{1\text{-}6}{\cdot}(H_2SO_4)_{3\text{-}7}{\cdot}HSO_4^-$), malonic acid-derived (MA-derived; including $C_3H_3O_4^-$, $C_3H_4O_4{\cdot}NO_3^-$, and $C_3H_4O_4{\cdot}HSO_4^-$), oxidized organic molecules ($CHO/CHON{\cdot}(HSO_4^-/NO_3^-)$), others (other identified negative ions, such as IO_3^-), and unidentified ions. The campaign-average diurnal variations of these eight negative ion groups are shown in Figure 4. Different diurnal patterns of each negative ion group were observed, mainly due to changes in concentrations of the parent neutral species and their unique physicochemical properties (e.g., the EA and PA of molecules; Ferguson and Arnold, 1981; Bianchi et al., 2017; Hirsikko et al., 2011).

$(HNO_3)_{0-1}\cdot NO_3^-$ and $(H_2SO_4)_{0-3}\cdot HSO_4^-$ were among the highest in the signal of all negative ion groups in all seasons, making up 37 % (whole day) and 20 % (daytime; 07:00 – 19:00, and hereafter) of negative ions at CHC during the study period, respectively. The EA of their neutral molecules (HSO_4 and NO_3) is higher than that of most of the neutral species in the atmosphere, and thus hinders the direct electron transfer from HSO_4^- and NO_3^- to other molecules through ion-molecule reactions (Ferguson and Arnold, 1981). As a result, these ion groups were found to dominate negative cluster ions at CHC and also other locations, such as a number of remote sites in the United States (Eisele, 1986), a boreal forest site in Finland (Ehn et al., 2010; Bianchi et al., 2017), and the JFJ in Switzerland (Frege et al., 2017).

Distinct diurnal patterns were observed for the $(HNO_3)_{0-1}\cdot NO_3^-$ and $(H_2SO_4)_{0-3}\cdot HSO_4^-$ ion groups. $(HNO_3)_{0-1}\cdot NO_3^-$ exhibited a relatively flat diurnal pattern (see Fig. 4) with similar fractions at daytime (35 %) and nighttime (19:00 – 07:00; 39 %). Such a diurnal pattern could result from the high EA of the NO_3 molecule (4.01 eV and an additional ~1 eV per HNO_3; Ferguson and Arnold, 1981), and its relatively abundant (usually several ppbv) parent neutral species (e.g., HNO_3 and N_2O_5) with multiple sources in the atmosphere (e.g., anthropogenic emission and lightning; Martin et al., 2007). In contrast, $(H_2SO_4)_{0-3}\cdot HSO_4^-$ exhibited a strong diurnal variation. While the fraction of $(H_2SO_4)_{0-3}\cdot HSO_4^-$ remained low (2 %) during nighttime, it started to increase after sunrise (shortly after 07:00) and reached a maximum (30 %) at around 10:00. Despite an EA comparable to that of the NO_3 molecule (4.75 eV for HSO_4; Wang et al., 2000), the strong diurnal variation of $(H_2SO_4)_{0-3}\cdot HSO_4^-$ is a result of the photochemical production of neutral H_2SO_4. The influence of neutral H_2SO_4 on $(H_2SO_4)_{0-3}\cdot HSO_4^-$ is indicated by their similar diurnal patterns (R: 0.52; see Fig. S4a). Similarly, a higher level of $(NH_3)_{1-6}\cdot(H_2SO_4)_{3-7}\cdot HSO_4^-$ was only observed with the presence of abundant $(H_2SO_4)_{0-3}\cdot HSO_4^-$ during daytime. It is also important to note that the decreases of $(H_2SO_4)_{0-3}\cdot HSO_4^-$ and $(NH_3)_{1-6}\cdot(H_2SO_4)_{3-7}\cdot HSO_4^-$ at around noontime (12:00; see Fig. 4) coincided with an enhanced CS, indicating the influence of a higher ion sink in addition to the decrease in neutral H_2SO_4 concentration (Boulon et al., 2010; Frege et al., 2017).

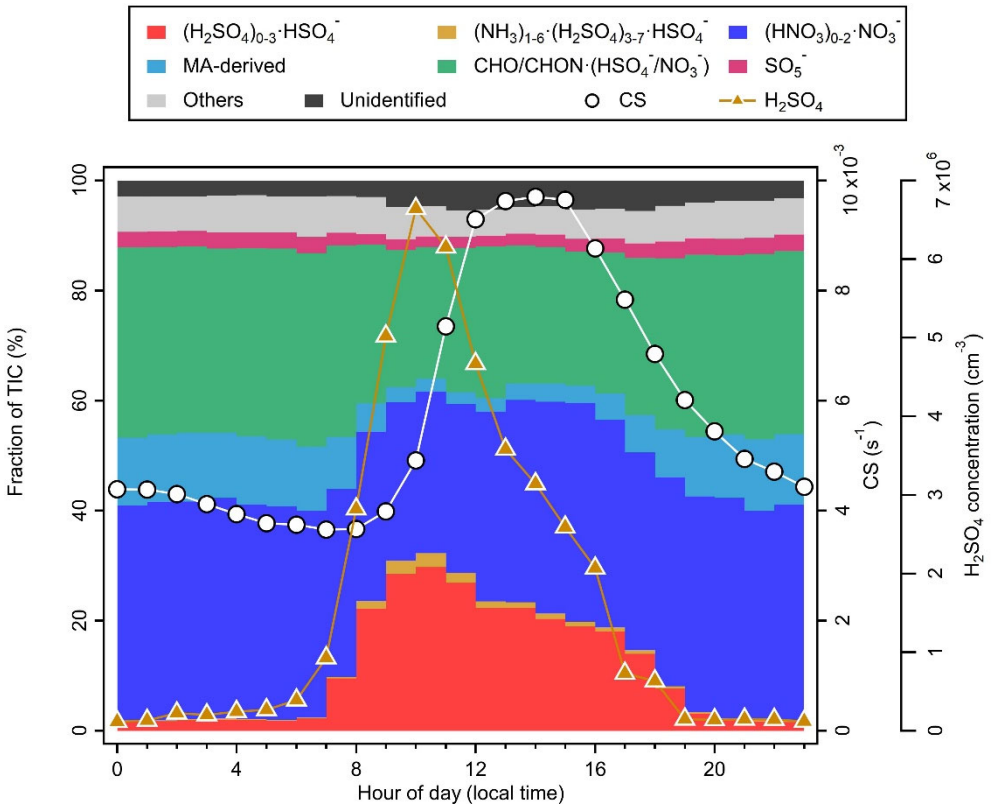

Figure 4 Diurnal variation of the negative ions (fraction of TIC), CS, and neutral H_2SO_4 concentrations at CHC, averaged over the periods when negative ions were measured (i.e., January, April, and May 2018).

The MA-derived ion group is distinguished from the CHO/CHON·(HSO_4^-/NO_3^-) ion group due to its abundance in total organic ions. This group of ions, mainly composed of $C_3H_3O_4^-$, is formed from the deprotonation of malonic acid, with a higher EA (~4.60 eV) than that of the NO_3 molecule (4.01 eV; Ravi Kumar et al., 2005). Malonic acid, similar to HNO_3, has multiple origins in the atmosphere, such as primary and secondary anthropogenic sources, biogenic sources, and the degradation of larger organic compounds (Braban et al., 2003). It is also one of the main dicarboxylic acids which make up a substantial fraction of total carbon in aerosol particles (Kawamura and Bikkina, 2016). However, the concentration of gas-phase malonic acid is less well documented and is estimated to be in the range of 10^7 to 10^9 cm^{-3}, up to three orders of magnitude higher than the typically reported ambient H_2SO_4 concentration (Fang et al., 2020). Thus, the fraction of the MA-derived ion group was high during nighttime (12 %; see Fig. 4). In contrast, its fraction decreased significantly (to 5 %) during daytime due to the increase of $(H_2SO_4)_{0-3}\cdot HSO_4^-$, which has an even higher EA (4.75 eV for HSO_4; Wang et al., 2000).

The CHO/CHON·(HSO_4^-/NO_3^-) ion group, with an overall molecular formula of $C_{2-15}H_{2-26}O_{2-13}N_{0-2}\cdot NO_3^-/HSO_4^-$, constituted a significant fraction of negative ions (31 %) at CHC. These organic ions are formed through the adduction between primary charge

carriers, such as HSO_4^- and NO_3^-, and neutral OOM. These OOM are likely the oxidation products of the volatile organic compounds (VOC) from the Amazon, the Altiplano, and the adjacent La Paz – El Alto metropolitan area. Their chemical composition is potentially affected by the changing air pathways covering different VOC source regions (Aliaga et al., 2021), and by the different conditions during daytime/nighttime due to the evolution of different atmospheric layers (Beck et al., 2022). While the diurnal variation was relatively small (34 % for the nighttime and 27 % for the daytime), the ion composition of CHO/CHON·(HSO_4^-/NO_3^-) could also be significantly different between daytime and nighttime due to the availability of the charging ions (see more discussions in Section 3.2.2). A previous study from a boreal forest shows that organic ions are mainly composed of CHO/CHON·NO_3^- during nighttime, and that the fraction of CHO/CHON·HSO_4^- increases with the HSO_4^- signal during daytime (Bianchi et al., 2017). This is also shown by the slightly positive correlation between the CHO/CHON·HSO_4^- signal fraction and the total neutral OOM concentration during daytime (*R*: 0.25; see Fig. S4b), whereas no clear dependence was found between CHO/CHON·(HSO_4^-/NO_3^-) and the total neutral OOM concentration.

The SO_5^- ion group, consisting of SO_5^- ions and/or O_2·SO_3^- cluster ions (Bork et al., 2013; Frege et al., 2017), exhibited a lower fraction (<5 %) than the aforementioned ion groups during the study period. Similar to that of the $(HNO_3)_{0\text{-}1}$·NO_3^- ion group, no diurnal pattern was evident for the SO_5^- ion group. This may be the result of its different major formation pathways during daytime and nighttime (Bork et al., 2013; Frege et al., 2017). Daytime production of SO_5^- ions is likely associated with photo-oxidation of SO_2 (similar to the formation pathway of H_2SO_4; Ehn et al., 2010; Schobesberger et al., 2015). This is shown in the positive correlation (*R*: 0.46 for daytime data in Fig. S4c) between the neutral H_2SO_4 concentration and the signal fraction of the SO_5^- ion group. During nighttime, however, the SO_5^- ion group is mainly composed of O_2 ·SO_3^- cluster ions, which are possibly formed via the oxidation of SO_2 with O_3^- (producing SO_3^-), and subsequent addition of O_2 (Bork et al., 2013).

3.2.2 Seasonalities of negative ions

For better seasonality comparison at high-altitude CHC, we calculated the average mass spectra of the negative ion groups for each season (Fig. 5 for daytime and Fig. S5 for nighttime). Distinct seasonalities (wet season, wet-to-dry transition period, and dry season) were found for the majority of the negative ion groups at CHC, including $(H_2SO_4)_{0\text{-}3}$·HSO_4^-, $(NH_3)_{1\text{-}6}$·$(H_2SO_4)_{3\text{-}7}$·HSO_4^-, SO_5^-, and organic cluster ions, as shown in the averaged daytime mass spectra (Fig. 5; more detailed reason will be discussed below). However, the signals of some other negative ion groups, e.g., MA-derived ions and $(HNO_3)_{0\text{-}2}$·NO_3^-, were generally stable (with differences ≤ 20 %) across the seasons. Such unclear seasonalities can be attributed to the high EA (Ferguson and Arnold, 1981; Ravi Kumar et al., 2005) and/or the stability of the parent neutral species (Martin et al., 2007; Kerminen et al., 2000; Bikkina et al., 2021). Similar patterns can also be found

in the average nighttime mass spectra among the seasons (Fig. S5).

$(H_2SO_4)_{0\text{-}3}{\cdot}HSO_4^-$ group exhibited much higher contribution in dry season (May) than in wet season (January) and wet-to-dry transition period (April). The daytime fraction of $(H_2SO_4)_{0\text{-}3}{\cdot}HSO_4^-$ increased continuously from 16 % in wet, 20 % in wet-to-dry transition period, to 30 % in dry season. The maximum number of H_2SO_4 molecules increased concurrently from 2 to 4 in the cluster ions (i.e., from $(H_2SO_4)_2{\cdot}HSO_4^-$ to $(H_2SO_4)_4{\cdot}HSO_4^-$). Similar trends were also found for other H_2SO_4-related ions, such as the $(NH_3)_{1\text{-}6}{\cdot}(H_2SO_4)_{3\text{-}7}{\cdot}HSO_4^-$ and SO_5^- during daytime (Fig. 5).

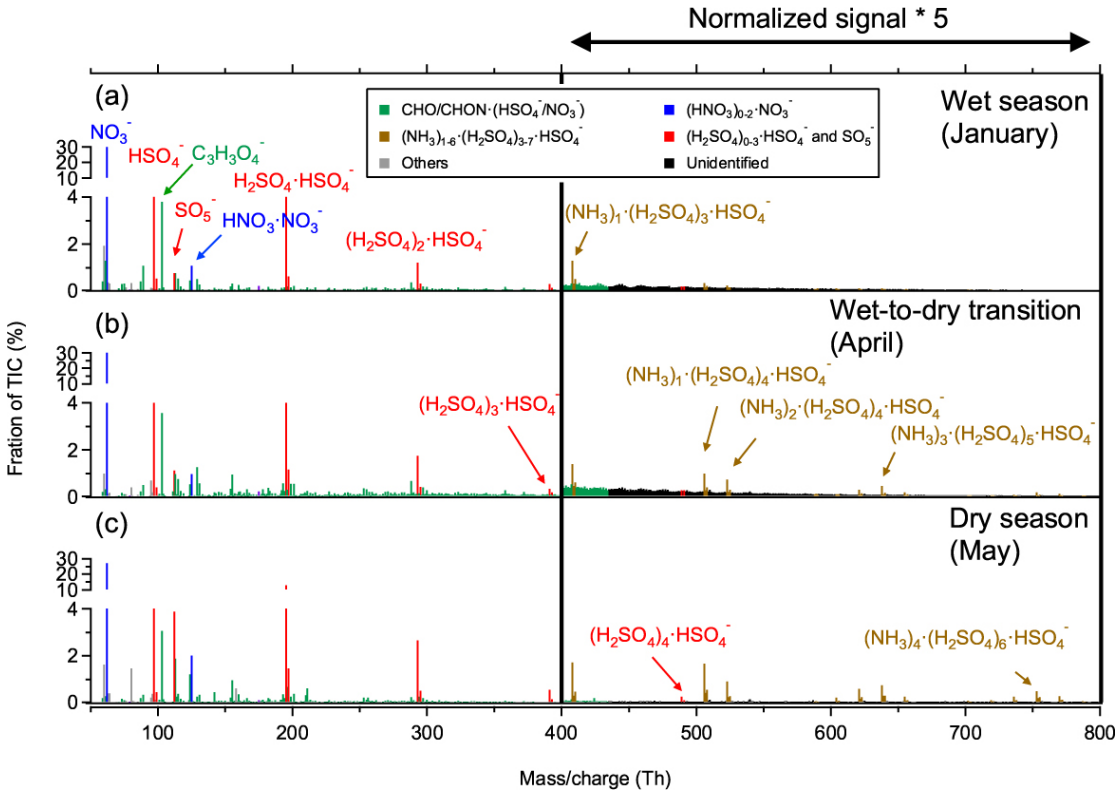

Figure 5 Mass spectra of negative ions at CHC averaged between 07:00 – 19:00 in **(a)** wet season (January), **(b)** wet-to-dry transition period (April), and **(c)** dry season (May). The normalized signal intensities from 400 Th to 800 Th are multiplied by a factor of 5 for better visualization.

The seasonal variations of the aforementioned H_2SO_4-related ion groups are likely due to the changes in neutral H_2SO_4 (Fig. S6) linked to the changing synoptic-scale wind patterns carrying different air masses with varying SO_2 (Bianchi et al., 2022). The air mass pathways 07_PW and 08_PW, covering the Western and Northern Altiplano plateau (see Table 1 and Fig. 2a), where active volcanic degassing of SO_2 has been reported (Moussallam et al., 2017; Carn et al., 2017), had their largest influence on CHC in dry season (i.e., May; see Fig. 2). The corresponding daytime fractions of $(H_2SO_4)_{0\text{-}3}{\cdot}HSO_4^-$ from these two pathways (Fig. 6a) were also the highest (27 % and 32 %, respectively). In contrast, air mass pathways 03_PW and 12_PW, originating in the Amazon Basin and Eastern/South-Eastern Lowlands, exerted their most significant

impact on CHC in wet season (i.e., January) with lower daytime fractions of $(H_2SO_4)_{0-3}{\cdot}HSO_4^-$ (13 % and 14 %, respectively). The low fractions of H_2SO_4-related cluster ions in wet season are also consistent with the lower SO_2 level in the Amazon Basin compared to the Altiplano plateau (Andreae et al., 1990). As for the wet-to-dry transition period (i.e., April), 05_PW covering both the South-Eastern Lowlands and Southern Altiplano plateau (where volcanic degassing is also significant; Carn et al., 2017) had an evident influence on CHC, resulting in a substantial level of H_2SO_4-related cluster ions (21 % for daytime). It is also noted that, because of the much lower nocturnal neutral H_2SO_4 concentrations, the nighttime fractions of H_2SO_4-related cluster ions in all air mass pathways (Fig. 6b) were generally low (< 3 %) and no clear seasonality was found.

The organic cluster ion group exhibited a distinct seasonal variation than the $(H_2SO_4)_{0-3}{\cdot}HSO_4^-$. The signal fraction of organic cluster ions was higher in wet season (31 % for daytime and 32 % for nighttime) than in dry season (23 % for daytime and 27 % for nighttime; Fig. 5 and Fig. S5), but it was highest for the wet-to-dry transition period (46 % for daytime and 52 % for nighttime; see Fig. 6).

The seasonal changes of organic cluster ions could be due to the combined effect of different meteorological conditions and VOC from different air mass origins (see Fig. 2). The air masses that originated from the Amazon Basin and Lowlands (03_PW and 12_PW) showed their largest impact on CHC in wet season (i.e., January). They contained higher fractions of organic cluster ions, which were 35 % and 34 % for daytime, and 50 % and 45 % for nighttime, respectively (Fig. 6). In dry season (i.e., May), however, the changes in air mass origin towards the Altiplano plateau and the Pacific Ocean led to a lower content of organic cluster ions. The organic cluster ion fractions for 07_PW and 08_PW (largest influence on CHC in dry season) in May were 23 % and 19 % for daytime, and 29 % and 27 % for nighttime, respectively. As for the wet-to-dry transition period (i.e., April), due to the combined influences of biogenic and anthropogenic VOC sources from 05_PW (evident impact on CHC in April), covering the South-Eastern Lowlands and the Southern Altiplano plateau, the corresponding organic cluster ion fractions from this air mass pathway were also the highest (41 % for daytime and 53 % for nighttime; see Fig. 6).

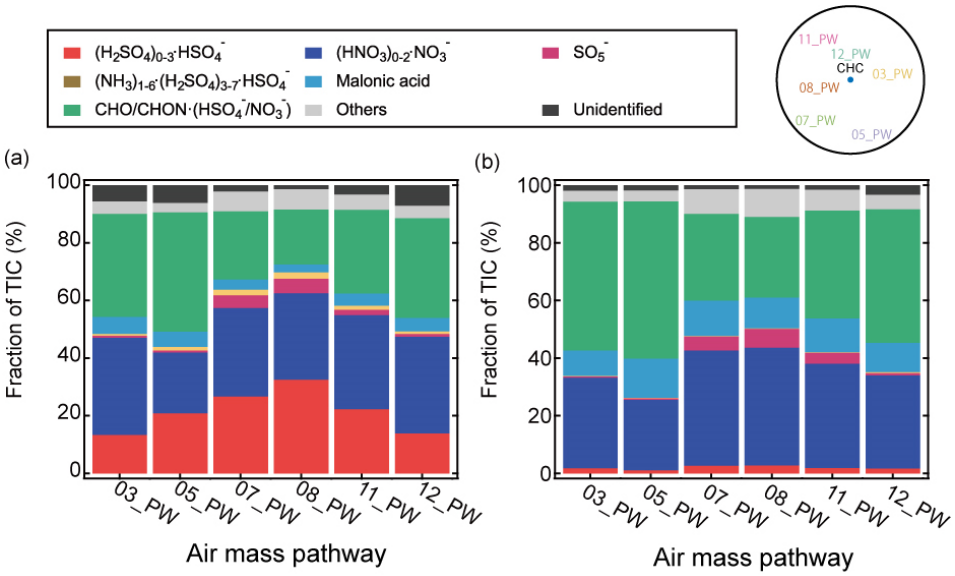

Figure 6 The fractions of the negative ion groups observed at CHC determined during the representative periods of each air mass pathway (described in Section 2.3.2) for **(a)** daytime (07:00 – 19:00) and **(b)** nighttime (19:00 – 07:00). A sketch of the horizontal profile of the air mass pathways (Fig. 2a) is shown in the upper right corner for clarity.

A further investigation of the organic ion group shows that the seasonal trends of the individual organic ions also varied (Fig. 7 for daytime and Fig. S7 for nighttime). Whereas the majority of the organic cluster ions at CHC were more abundant during wet season (Fig. 7a and Fig. S7a), fractions of CHO/CHON·HSO_4^- increased during the dry season. The observed increases of CHO/CHON·HSO_4^- cluster ions could be associated with the increased HSO_4^-/NO_3^- ratios in dry season (Fig. 5 and Fig. S5). Similar increases of CHO/CHON·HSO_4^- cluster ions were also found to relate to the ratio of HSO_4^-/NO_3^- in a boreal forest environment (Bianchi et al., 2017). In addition, changes in OOM composition between wet and dry seasons may also play a role (Fig. 7b and Fig. S7b), as NO_3^- tends to cluster with OOM containing hydroxyl and hydroperoxyl functional groups (Hyttinen et al., 2015) while some other observed OOM may be more efficiently charged by HSO_4^-.

The seasonal variations of the individual organic cluster ions are likely caused by different air masses (Fig. 7b and Fig. S7b). The air masses influenced by tropical rainforest vegetation from the Amazon Basin are dominated by isoprene (C_5H_8) emissions and isoprene oxidation products (Bianchi et al., 2022). This region corresponds to 03_PW and 12_PW (largest impact on CHC in wet season in January) consisting of relatively higher fractions of organic cluster ions with OOM containing 4-5 carbon atoms (50 % and 46 % for nighttime, and 29 % and 32 % for daytime, respectively). In contrast, when the air masses were more influenced by the Altiplano plateau (i.e., 05_PW, 07_PW, and 08_PW, with more anthropogenic emissions and less vegetation) in wet-to-dry transition period and dry season, organic cluster ions with 6-8 carbon atoms, potentially originating from anthropogenic sources (e.g., toluene

(C_7H_8); Huang et al., 2019; Cai et al., 2022), were of higher contributions. The signal fractions of these organic ions were thus the highest in these air mass pathways, accounting for 36-39 % for nighttime and 37-39 % for daytime. For all the air mass pathways, fractions of organic ions with more than 9 carbon atoms were relatively low (<10 %). This might be due to their lower volatilities compared to OOM with smaller carbon numbers (Donahue et al., 2012), resulting in a larger probability of them being removed during their transport to CHC (e.g., condensing on pre-existing particles).

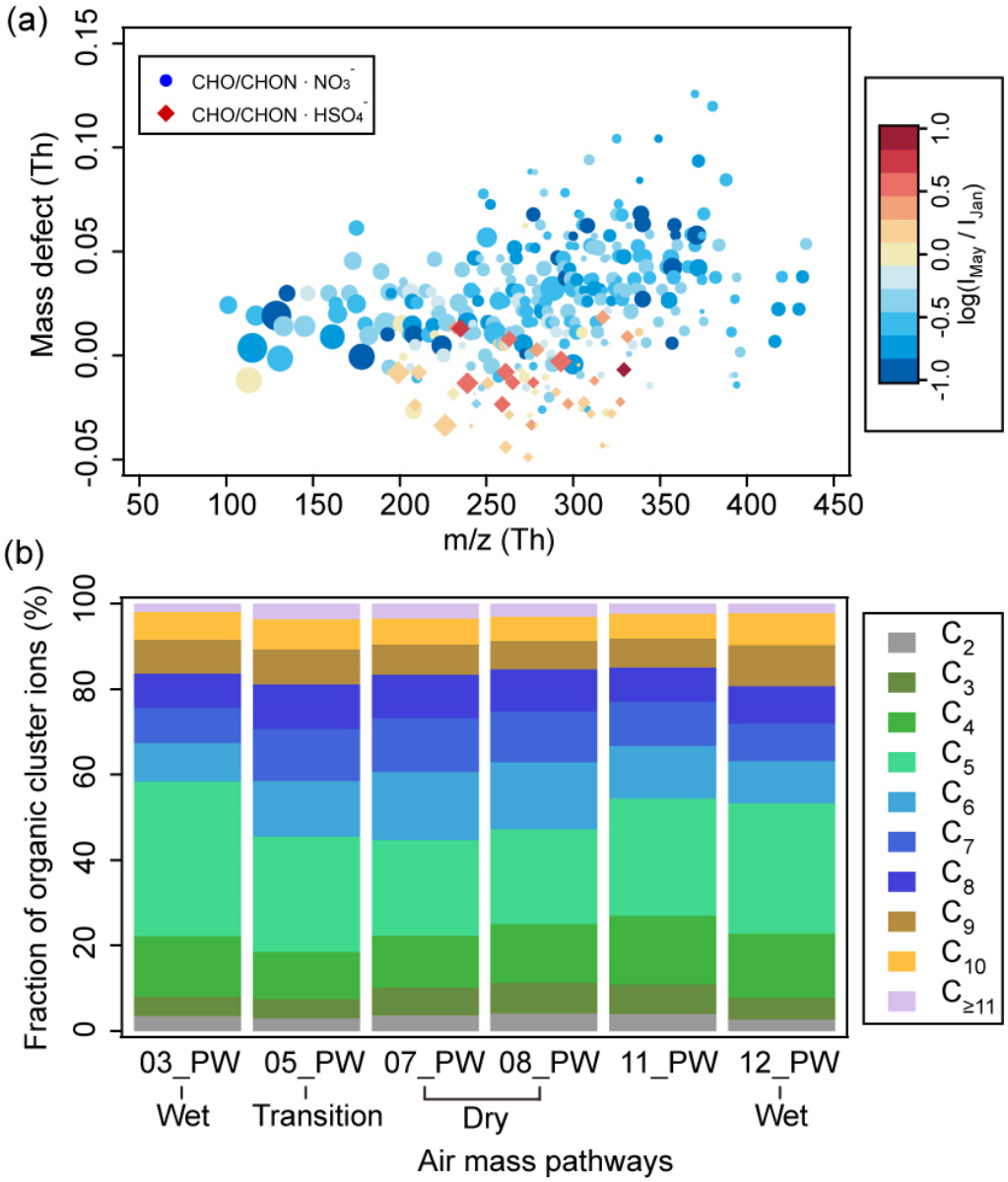

Figure 7 **(a)** Mass defect plot of organic cluster ions during nighttime (19:00-07:00). The color code indicates ratios (in log scale) between median signals of each ion detected in May (IMay) of dry season and January (IJan) of wet season. The marker size is proportional to the log-transformed median signals of ions in May. **(b)** Fraction of organic cluster ions from different air mass pathways as a function of carbon atom numbers during nighttime (19:00-07:00). A similar figure based on daytime data (07:00-19:00) is in the supplementary information (Figure S7). Note that MA-derived

ions were not included in this figure.

3.3 Positive ions

Several positive cluster ion groups were consistently observed in February and March (i.e., wet season) during the study period. Based on their chemical composition, the positive cluster ions measured at CHC are classified into four groups (Fig. 8): (1) a series of protonated amines, including trimethylamine ($C_3H_9N{\cdot}H^+$), pyridine ($C_5H_7N{\cdot}H^+$), aniline ($C_6H_7N{\cdot}H^+$), and benzylamine ($C_7H_9\ N{\cdot}H^+$); (2) organic cluster ions consisting of OOM (identified as $C_{3\text{-}24}H_{6\text{-}39}O_{2\text{-}12}N_{0\text{-}2}$) clustered with positive charge carriers such as protons (H^+), ammonium (NH_4^+), and aminium (NH^+) ions; (3) contamination ions; and (4) unidentified ions (likely organic ions in higher masses; Bianchi et al., 2021). Contamination in the positive cluster ions includes ethylhexylglycerin (e.g., $C_{11}H_{24}O_3{\cdot}NH^+$), which is widely used in cosmetics (Aerts et al., 2016), and polydimethylsiloxane (e.g., $(C_2H_6OSi)_7{\cdot}NH_4^+$) possibly from instrument tubing (Bianchi et al., 2014). In contrast to the negative cluster ions, the four positive cluster ion groups were generally stable with smaller diurnal variability over the study period (Fig. 9). This is similar to the diurnal patterns determined in previous studies in a boreal forest environment (Ehn et al., 2010) and at the JFJ (Frege et al., 2017). However, due to the unavailable measurements of the corresponding neutral species (e.g., amines), the exact reason for such weak diurnal variations observed in different locations remains unclear.

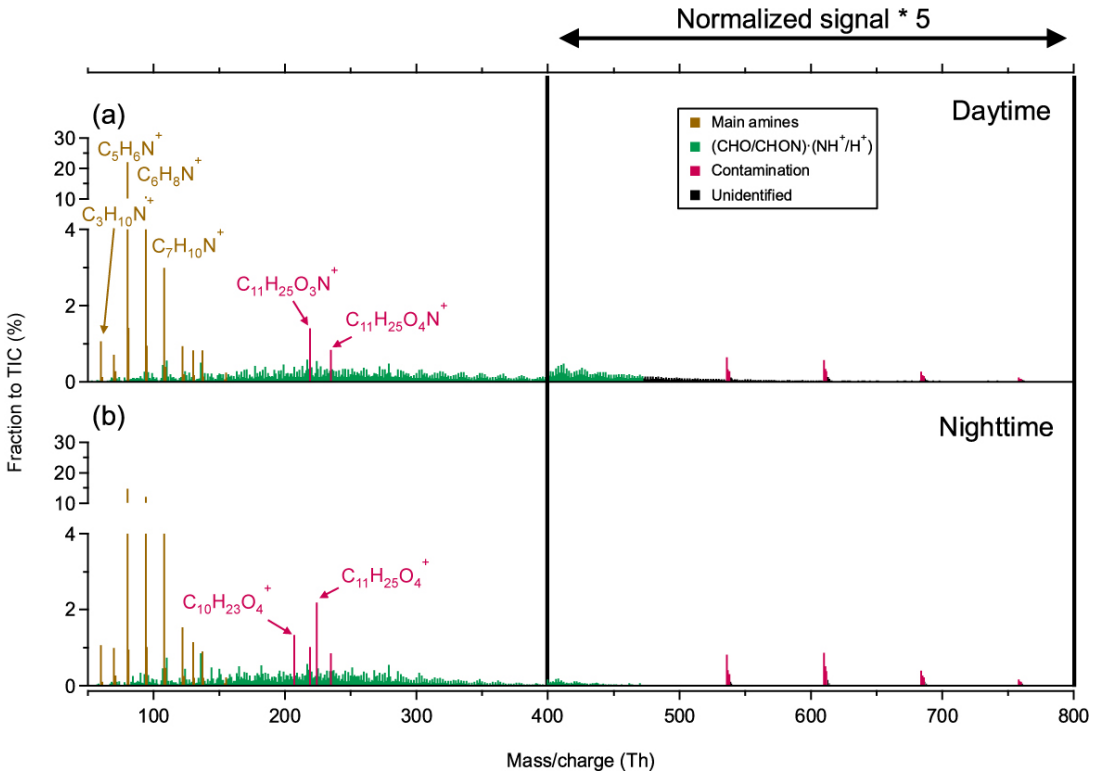

Figure 8 Averaged mass spectra of positive ions at CHC in February and March 2018 when APi-TOF was operating in positive ion mode (see section 2.2.1), during **(a)**

daytime (07:00 – 19:00) and **(b)** nighttime (19:00 – 07:00). The normalized signal intensities from 400 Th to 800 Th are multiplied by a factor of 5 for better visualization.

The protonated amines were the most abundant positive ion group (46 %), with no significant diurnal variations. Nighttime contributions of this ion group (47 %) were similar to its daytime contributions (45 %; Fig. 9). They also dominated the positive ion spectra observed in different environments, such as a boreal forest (Ehn et al., 2010), the JFJ (Frege et al., 2017), and the free troposphere (Schulte and Arnold, 1990). Their sources have not been fully identified (Kosyakov et al., 2020), but they are widely used as solvents and dyes (Sims et al., 1989), which may be potential sources of these ions observed at CHC.

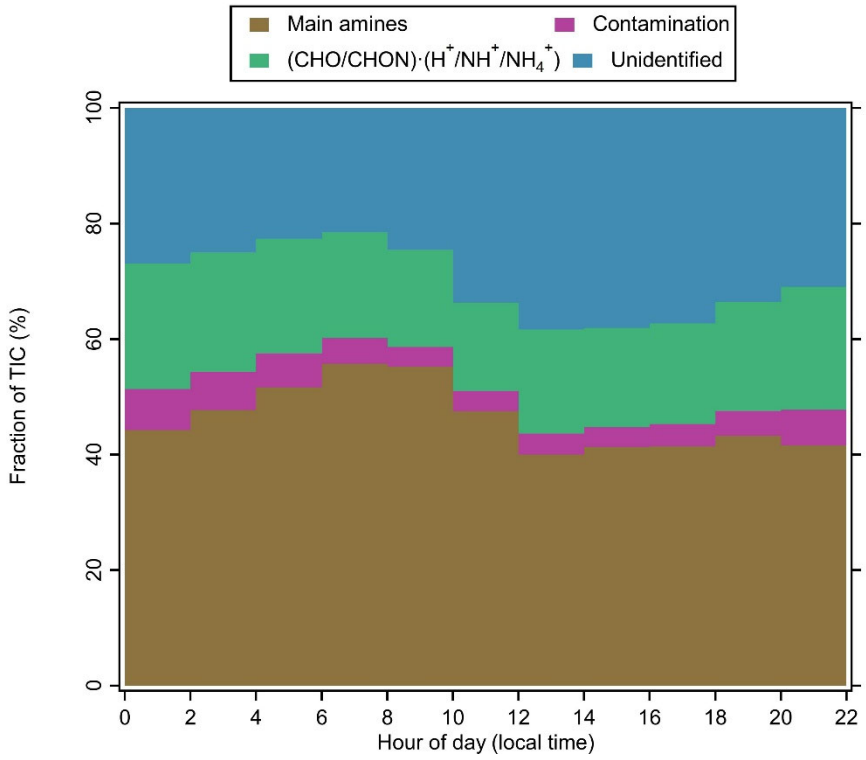

Figure 9 Diurnal variation of positive ion groups at CHC, averaged over measurements in February and March 2018 (when APi-TOF was operating in positive ion mode, see section 2.2.1).

Positive organic cluster ions were also relatively abundant (19 %) at CHC during the wet season. Similar to the negative organic ions in wet season (Fig. 6), this reflects the influence of air masses originating from the Amazon Basin and Eastern/South-Eastern Lowlands (e.g., 03_PW and 11_PW). Differences in the positive organic ion signals between nighttime (21 %) and daytime (18 %) were small, which is similar to the negative organic cluster ions (see Fig. 3). A further investigation of the relationship between these positive ions and their neutral species is, unfortunately, not possible due to the unavailability of CI-APi-TOF data in February and March caused by instrumental issues.

3.4 Potential connections between atmospheric ions and new particle formation events

During the SALTENA campaign from January to May 2018, NPF events were frequently observed at CHC (Fig. S8). While most of them occurred from April (the wet-to-dry transition period, 21 events) to May (dry season, 26 events), NPF events seldom occurred during wet season from January to March (8 events in total). This is consistent with a previous study performed at CHC (Rose et al., 2015a), which also found that NPF events mainly occurred during dry season.

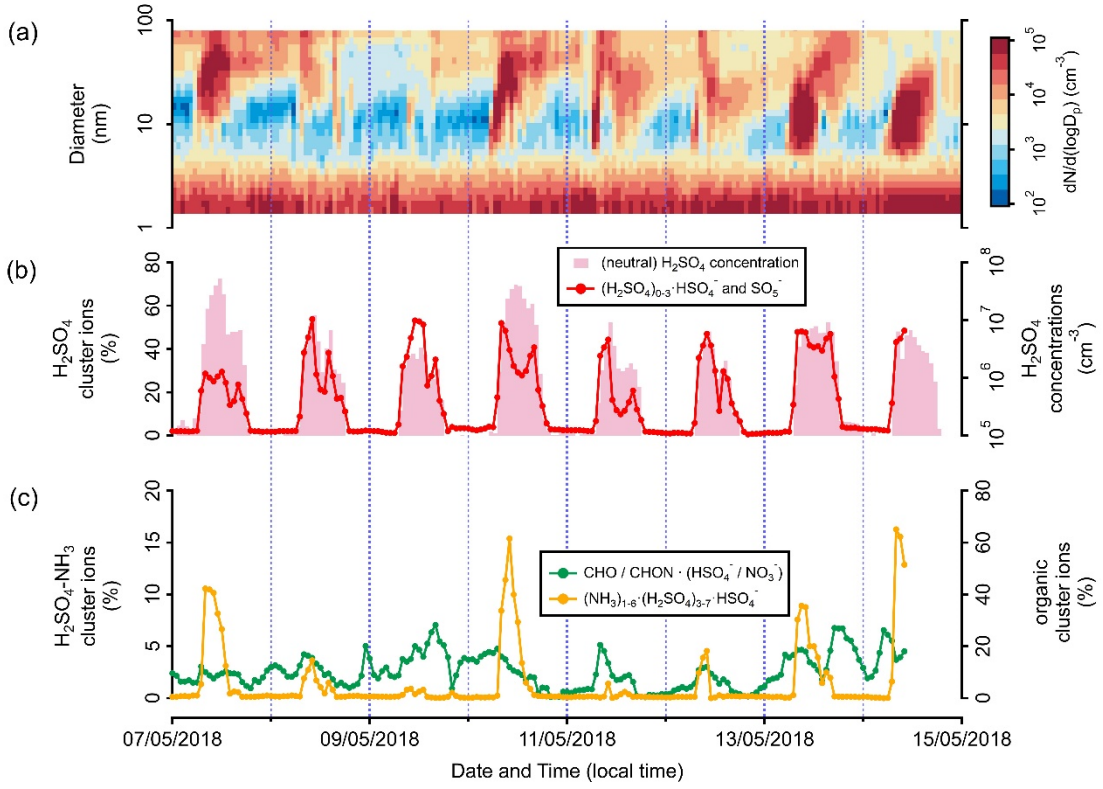

Figure 10 Time series of the **(a)** size distribution of aerosol particles (measured with NAIS and MPSS), (**b**) signal fraction of the $(H_2SO_4)_{0\text{-}3}{\cdot}HSO_4^-$ ion group and neutral H_2SO_4 concentration, and **(c)** signal fractions of the $(NH_3)_{1\text{-}6}{\cdot}(H_2SO_4)_{3\text{-}7}{\cdot}HSO_4^-$ and negative organic cluster ion groups, observed at CHC from 7 to 14 May 2018 when NPF occurred frequently.

Previous field studies at high-altitude mountain sites have shown that NPF events can be triggered by different compounds, such as low-volatile neutral OOM (Bianchi et al., 2021), neutral H_2SO_4 and OOM (Bianchi et al., 2016), and H_2SO_4-NH_3 cluster ions (Frege et al., 2017). While the signal fractions of the negative organic cluster ions did not seem to have a strong correlation with the onset of the NPF events, the fractions of the $(NH_3)_{1\text{-}6}{\cdot}(H_2SO_4)_{3\text{-}7}{\cdot}HSO_4^-$ (associated with $(H_2SO_4)_{0\text{-}3}{\cdot}HSO_4^-$) always increased concurrently with the number concentration of small particles (see example NPF events on, e.g., 7, 10, 13, and 14 May 2018; Fig. 10). The number of NPF days increased when

more H_2SO_4 molecules were present in the $(NH_3)_{1-6}{\cdot}(H_2SO_4)_{3-7}{\cdot}HSO_4^-$ cluster ion (Fig. 11a). In particular, more than half of the NPF events (28 out of the total 55 events) were observed in the presence of $(NH_3)_{4-6}{\cdot}(H_2SO_4)_7{\cdot}HSO_4^-$. The majority (35 events) of all the NPF events exhibited clear nucleation and growth processes (i.e., Class 1 events; the classification is defined following the approach by Yli-Juuti et al. (2009); Fig. 11b). In contrast, only Class 2 (similar to Class 1 but with less clarity) and bump events (early growth of the newly formed particles is interrupted) were observed when only $(H_2SO_4)_2{\cdot}HSO_4^-$ was observed.

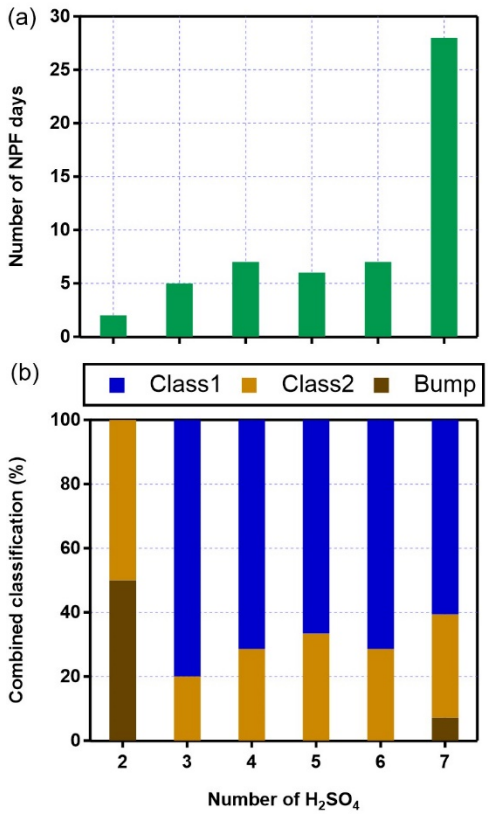

Figure 11 Connection between the maximum number of H_2SO_4 (in addition to HSO_4^-) observed in the $(H_2SO_4)_2{\cdot}HSO_4^-$ and $(NH_3)_{1-6}{\cdot}(H_2SO_4)_{3-7}{\cdot}HSO_4^-$ cluster ions during NPF events and **(a)** the number of NPF days; **(b)** proportions of different NPF classes.

Moreover, higher levels (up to an order of magnitude) of $(NH_3)_{1-6}{\cdot}(H_2SO_4)_{3-7}{\cdot}HSO_4^-$ and $(H_2SO_4)_{0-3}{\cdot}HSO_4^-$ ions as well as negative organic cluster ions charged by HSO_4^- were also observed during the NPF days (Fig. 12). In contrast, other negative ion groups (e.g., the majority of the negative organic cluster ions charged by NO_3^-) were more abundant during the non-NPF days. Our observations indicate a potentially important role of $(NH_3)_{1-6}{\cdot}(H_2SO_4)_{3-7}{\cdot}HSO_4^-$ cluster ions in NPF events at CHC from January to May 2018, particularly in wet-to-dry transition period and dry season.

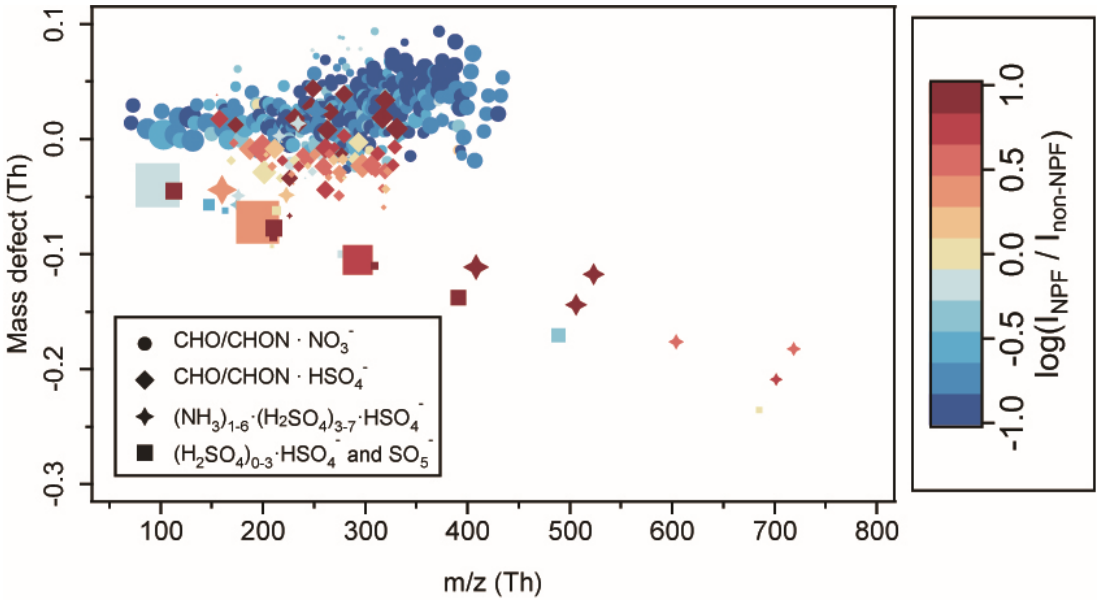

Figure 12 Mass defect plot of differences in negative cluster ion composition between NPF and non-NPF days. The negative ion composition of NPF events was averaged over all NPF days from 08:00 to 12:00 in January, April, and May 2018 (when APi-TOF was operating in negative ion mode, see section 2.2.1) at CHC. The ion composition of non-NPF days was averaged over non-NPF days from 08:00 to 12:00 for the same period. The x-axis is the exact mass of cluster ions, and the y-axis is the mass defect. The color code indicates ratios (in log scale) between median signals of each ion determined in NPF events (I_{NPF}) and non-NPF periods ($I_{non\text{-}NPF}$). The marker size is proportional to the log-transformed median signals of ions observed in the NPF events that occurred in January, April and May. Note that $(HNO_3)_{0\text{-}2}{\cdot}NO_3^-$ cluster ions were not included here.

The majority of the observed NPF events occurred when CHC was more impacted by air masses originating from source regions with elevated SO_2 emissions (05_PW, 07_PW, and 08_PW). This is similar to the observations from the high-altitude station JFJ (Frege et al., 2017). Moreover, consistent with the previous findings from Rose et al. (2015a), CHC was affected by the frequent arrival of air masses from the Pacific Ocean during the dry season (see also Fig. 2). And the NPF during the dry season at CHC seems to be triggered once the air masses arrive on the continent (Rose et al., 2015). However, these air masses of marine origin may not directly contain the nucleating species (also reflected in the poor connection between NPF events and the levels of methanesulfonic acid ion ($CH_3SO_3^-$) or IO_3^-; data not shown). In addition, inconsistent time series of $CH_3SO_3^-$ and IO_3^- prohibit us from drawing further conclusions on the role of marine-derived compounds on NPF at Chacaltaya during the dry season. In addition, the fraction of large positive organic cluster ions (mass range from 500 to 800 Th; Fig. S9) was found to increase during the NPF events in the wet season. These organic cluster ions usually contained at least ten carbon atoms (Fig. S10). Such large positive organic ions have been found to contribute to NPF in the Himalayas (Bianchi et al., 2021), and thus, their contribution to NPF can not be completely ruled

out at CHC as well.

4. Conclusion

In this study, both negative and positive atmospheric ions were measured at a high-altitude research station (CHC) in the Bolivian Andes for five months, from January to May 2018, using an APi-TOF mass spectrometer. Negative ions were mainly composed of $(H_2SO_4)_{0\text{-}3}{\cdot}HSO_4^-$, $(HNO_3)_{0\text{-}2}{\cdot}NO_3^-$, SO_5^-, $(NH_3)_{1\text{-}6}{\cdot}(H_2SO_4)_{3\text{-}7}{\cdot}HSO_4^-$, MA-derived, and CHO/CHON·(HSO_4^-/NO_3^-) ion groups. Positive ions mainly consisted of a series of protonated amines ($C_{3\text{-}7}H_{7\text{-}9}N{\cdot}H^+$) and organic cluster ions CHO/CHON·$(H^+/NH_4^+/NH^+)$. Distinct diurnal variation was observed for the negative ions, and attributed mainly to the changes in the corresponding neutral species' concentrations and/or their EA / PA. An example is H_2SO_4-related cluster ions, the diel temporal variation of which was mainly due to the photochemical production of neutral H_2SO_4 during daytime. Strong seasonality of negative ions was also found, such as for H_2SO_4-related cluster ions owing to changes in SO_2 and the resulting neutral H_2SO_4 concentrations. The seasonal variation was mainly because of the differences in source regions of air masses arriving at CHC from wet to dry seasons. In contrast, no significant diurnal variation was observed for the positive ions. The comparison between NPF and non-NPF days infers that H_2SO_4-NH_3 cluster ions contribute to the aerosol nucleation process at CHC, particularly in wet-to-dry transition period and dry season when CHC was more impacted by air masses originating from source regions with elevated SO_2 emissions. The results further indicate that atmospheric ion composition at CHC is directly affected by air masses from different source regions.

Measurements of atmospheric ions in the field will improve understanding of atmospheric physical and chemical processes in the study regions, as the ions play important roles in atmospheric chemistry through participation in or catalysis of ion-molecule reactions and ion-induced new particle formation. Our study thus provides new insights into the chemical composition of atmospheric ions and their potential role in high-altitude NPF in the Bolivian Andes where both natural (e.g., biogenic and volcanic) and anthropogenic emissions are important.

Data availability: The data that are involved in the figures can be found in doi.org/10.5281/zenodo.7271286 (Zha et al., 2022).

Author contributions: Q. Z., W.H., and F.B. analysed the data; D.A. conducted the air mass history analysis; Q.Z., W.H., F.B., D.A., O.P., L.H., A.M.K., C.W., J.E., Y.G., M.A., C.M., and F.B. collected the data and operated the instruments during the measurement campaign. Q.Z. and W.H. wrote the manuscript with contributions from J.C., V.S., S.C., D.W., R.K., M.A., C.M., and F.B. All authors commented on the manuscript.

Competing interests: The authors declare no competing interests.

Acknowledgment: We thank the Bolivian staff of the IIF-UMSA (Physics Research Institute, UMSA) working at CHC and the long-term observations performed within the framework of GAW and ACTRIS. We thank the IRD (Institut de Recherche pour le Développement) for the logistic and financial support during the campaign, including shipping and customs concerns. We thank the CSC-IT Center for Science, Finland, for the generous computational resources that allowed the WRF and FLEXPART-WRF simulations to be conducted.

Grant information: This research has received support from European Union (EU) H2020 program via the findings European Research Council (ERC; project CHAPAs no. 850614 and ATM-GTP no. 742206), the Marie Skłodowska Curie (CLOUD-MOTION no. 764991), the Finnish Centre of Excellence as well as the Academy of Finland (project no. 311932, 315203 and 337549), and the Knut and Alice Wallenberg Foundation (WAF project CLOUDFORM no. 2017.0165).

Reference

Aerts, O., Verhulst, L., and Goossens, A.: Ethylhexylglycerin: a low-risk, but highly relevant, sensitizer in 'hypo-allergenic' cosmetics, Contact Dermatitis, 74, 281–288, 2016.

Aliaga, D., Sinclair, V. A., Andrade, M., Artaxo, P., Carbone, S., Kadantsev, E., Laj, P., Wiedensohler, A., Krejci, R., and Bianchi, F.: Identifying source regions of air masses sampled at the tropical high-altitude site of Chacaltaya using WRF-FLEXPART and cluster analysis, Atmos. Chem. Phys., 21, 16453–16477, 2021.

Andrade, M., Zaratti, F., Forno, R., Gutiérrez, R., Moreno, I., Velarde, F., Ávila, F., Roca, M., Sánchez, M., Laj, P., Jaffrezo, J., Ginot, P., Sellegri, K., Ramonet, M., Laurent, O., Weinhold, K., Wiedensohler, A., Krejci, R., Bonasoni, P., Cristofanelli, P., Whiteman, D., Vimeux, F., Dommergue, A., and Magand, O.: Puesta en marcha de una nueva estación de monitoreo climático en los andes centrales de Bolivia: la estación Gaw/Chacaltaya, Rev. Boliv. Física, 26, 06–15, 2015.

Andreae, M. O., Berresheim, H., Bingemer, H., Jacob, D. J., Lewis, B. L., Li, S.-M., and Talbot, R. W.: The atmospheric sulfur cycle over the Amazon Basin: 2. Wet season, J. Geophys. Res., 95, 16813, 1990.

Beck, L. J., Sarnela, N., Junninen, H., Hoppe, C. J. M., Garmash, O., Bianchi, F., Riva, M., Rose, C., Peräkylä, O., Wimmer, D., Kausiala, O., Jokinen, T., Ahonen, L., Mikkilä, J., Hakala, J., He, X.-C., Kontkanen, J., Wolf, K. K. E., Cappelletti, D., Mazzola, M., Traversi, R., Petroselli, C., Viola, A. P., Vitale, V., Lange, R., Massling, A., Nøjgaard, J. K., Krejci, R., Karlsson, L., Zieger, P., Jang, S., Lee, K., Vakkari, V., Lampilahti, J., Thakur, R. C., Leino, K., Kangasluoma, J., Duplissy, E.-M., Siivola, E., Marbouti, M., Tham, Y. J., Saiz-Lopez, A., Petäjä, T., Ehn, M., Worsnop, D. R., Skov, H., Kulmala, M., Kerminen, V.-M., and Sipilä, M.: Differing Mechanisms of New Particle Formation at Two Arctic Sites, Geophys. Res. Lett., 48, e2020GL091334, 2021.

Beck, L. J., Schobesberger, S., Junninen, H., Lampilahti, J., Manninen, A., Dada, L., Leino, K., He, X.-C., Pullinen, I., Quéléver, L. L. J., Franck, A., Poutanen, P., Wimmer, D., Korhonen, F., Sipilä, M., Ehn, M., Worsnop, D. R., Kerminen, V.-M., Petäjä, T., Kulmala, M., and Duplissy, J.: Diurnal evolution of negative atmospheric ions above the boreal forest: from ground level to the free troposphere, Atmos. Chem. Phys., 22, 8547–8577, 2022.

Bianchi, F., Praplan, A. P., Sarnela, N., Dommen, J., Kürten, A., Ortega, I. K., Schobesberger, S., Junninen, H., Simon, M., Tröstl, J., Jokinen, T., Sipilä, M., Adamov, A., Amorim, A., Almeida, J., Breitenlechner, M., Duplissy, J., Ehrhart, S., Flagan, R. C., Franchin, A., Hakala, J., Hansel, A., Heinritzi, M., Kangasluoma, J., Keskinen, H., Kim, J., Kirkby, J., Laaksonen, A., Lawler, M. J., Lehtipalo, K., Leiminger, M., Makhmutov, V., Mathot, S., Onnela, A., Petäjä, T., Riccobono, F., Rissanen, M. P., Rondo, L., Tomé, A., Virtanen, A., Viisanen, Y., Williamson, C., Wimmer, D., Winkler,

705 P. M., Ye, P., Curtius, J., Kulmala, M., Worsnop, D. R., Donahue, N. M., and
706 Baltensperger, U.: Insight into acid-base nucleation experiments by comparison of the
707 chemical composition of positive, negative, and neutral clusters, Environ. Sci. Technol.,
708 48, 13675–13684, 2014.

709 Bianchi, F., Tröstl, J., Junninen, H., Frege, C., Henne, S., Hoyle, C. R., Molteni, U.,
710 Herrmann, E., Adamov, A., Bukowiecki, N., Chen, X., Duplissy, J., Gysel, M., Hutterli,
711 M., Kangasluoma, J., Kontkanen, J., Kürten, A., Manninen, H. E., Münch, S., Peräkylä,
712 O., Petäjä, T., Rondo, L., Williamson, C., Weingartner, E., Curtius, J., Worsnop, D. R.,
713 Kulmala, M., Dommen, J., and Baltensperger, U.: New particle formation in the free
714 troposphere: A question of chemistry and timing., Science, 352, 1109–12, 2016.

715 Bianchi, F., Garmash, O., He, X., Yan, C., Iyer, S., Rosendahl, I., Xu, Z., Rissanen, M.
716 P., Riva, M., Taipale, R., Sarnela, N., Petäjä, T., Worsnop, D. R., Kulmala, M., Ehn, M.,
717 and Junninen, H.: The role of highly oxygenated molecules (HOMs) in determining the
718 composition of ambient ions in the boreal forest, Atmos. Chem. Phys., 17, 13819–
719 13831, 2017.

720 Bianchi, F., Junninen, H., Bigi, A., Sinclair, V. A., Dada, L., Hoyle, C. R., Zha, Q., Yao,
721 L., Ahonen, L. R., Bonasoni, P., Buenrostro Mazon, S., Hutterli, M., Laj, P., Lehtipalo,
722 K., Kangasluoma, J., Kerminen, V. M., Kontkanen, J., Marinoni, A., Mirme, S., Molteni,
723 U., Petäjä, T., Riva, M., Rose, C., Sellegri, K., Yan, C., Worsnop, D. R., Kulmala, M.,
724 Baltensperger, U., and Dommen, J.: Biogenic particles formed in the Himalaya as an
725 important source of free tropospheric aerosols, Nat. Geosci., 14, 4–9, 2021.

726 Bianchi, F., Sinclair, V. A., Aliaga, D., Zha, Q., Scholz, W., Wu, C., Heikkinen, L.,
727 Modini, R., Partoll, E., Velarde, F., Moreno, I., Gramlich, Y., Huang, W., Leiminger, M.,
728 Enroth, J., Peräkylä, O., Marinoni, A., Xuemeng, C., Blacutt, L., Forno, R., Gutierrez,
729 R., Ginot, P., Uzu, G., Facchini, M. C., Gilardoni, S., Gysel-Beer, M., Cai, R., Petäjä,
730 T., Rinaldi, M., Saathoff, H., Sellegri, K., Worsnop, D., Artaxo, P., Hansel, A., Kulmala,
731 M., Wiedensohler, A., Laj, P., Krejci, R., Carbone, S., Andrade, M., and Mohr, C.: The
732 SALTENA experiment: Comprehensive observations of aerosol sources, formation and
733 processes in the South American Andes, Bull. Am. Meteorol. Soc., 1, 1–46, 2022.

734 Bikkina, S., Kawamura, K., Sakamoto, Y., and Hirokawa, J.: Low molecular weight
735 dicarboxylic acids, oxocarboxylic acids and α-dicarbonyls as ozonolysis products of
736 isoprene: Implication for the gaseous-phase formation of secondary organic aerosols,
737 Sci. Total Environ., 769, 144472, 2021.

738 Bork, N., Kurtén, T., and Vehkamäki, H.: Exploring the atmospheric chemistry of
739 $O_2SO_3^-$ and assessing the maximum turnover number of ion-catalysed H_2SO_4 formation,
740 Atmos. Chem. Phys., 13, 3695–3703, 2013.

741 Boulon, J., Sellegri, K., Venzac, H., Picard, D., Weingartner, E., Wehrle, G., Collaud
742 Coen, M., Bütikofer, R., Flückiger, E., Baltensperger, U., and Laj, P.: New particle
743 formation and ultrafine charged aerosol climatology at a high altitude site in the Alps

(Jungfraujoch, 3580 m a.s.l., Switzerland), Atmospheric Chem. Phys., 10, 9333–9349, 2010.

Braban, C. F., Carroll, M. F., Styler, S. A., and Abbatt, J. P. D.: Phase Transitions of Malonic and Oxalic Acid Aerosols, J. Phys. Chem. A, 107, 6594–6602, 2003.

Brioude, J., Arnold, D., Stohl, A., Cassiani, M., Morton, D., Seibert, P., Angevine, W., Evan, S., Dingwell, A., Fast, J. D., Easter, R. C., Pisso, I., Burkhart, J., and Wotawa, G.: The Lagrangian particle dispersion model FLEXPART-WRF version 3.1, Geosci. Model Dev., 6, 1889–1904, 2013.

Cai, J., Wu, C., Wang, J., Du, W., Zheng, F., Hakala, S., Fan, X., Chu, B., Yao, L., Feng, Z., Liu, Y., Sun, Y., Zheng, J., Yan, C., Bianchi, F., Kulmala, M., Mohr, C., and Daellenbach, K. R.: Influence of organic aerosol molecular composition on particle absorptive properties in autumn Beijing, Atmospheric Chem. Phys., 22, 1251–1269, 2022.

Carn, S. A., Fioletov, V. E., McLinden, C. A., Li, C., and Krotkov, N. A.: A decade of global volcanic SO2 emissions measured from space, Sci. Rep., 7, 44095, 2017.

Chauvigné, A., Aliaga, D., Sellegri, K., Montoux, N., Krejci, R., Močnik, G., Moreno, I., Müller, T., Pandolfi, M., Velarde, F., Weinhold, K., Ginot, P., Wiedensohler, A., Andrade, M., and Laj, P.: Biomass burning and urban emission impacts in the Andes Cordillera region based on in situ measurements from the Chacaltaya observatory, Bolivia (5240 m a.s.l.), Atmos. Chem. Phys., 19, 14805–14824, 2019.

Donahue, N. M., Kroll, J. H., Pandis, S. N., and Robinson, A. L.: A two-dimensional volatility basis set – Part 2: Diagnostics of organic-aerosol evolution, Atmos. Chem. Phys., 12, 615–634, 2012.

Ehn, M., Junninen, H., Petäjä, T., Kurtén, T., Kerminen, V.-M., Schobesberger, S., Manninen, H. E., Ortega, I. K., Vehkamäki, H., Kulmala, M., and Worsnop, D. R.: Composition and temporal behavior of ambient ions in the boreal forest, Atmos. Chem. Phys., 10, 8513–8530, 2010.

Eisele, F. L.: Identification of tropospheric ions, J. Geophys. Res. Atmos., 91, 7897–7906, 1986.

Fang, X., Hu, M., Shang, D., Tang, R., Shi, L., Olenius, T., Wang, Y., Wang, H., Zhang, Z., Chen, S., Yu, X., Zhu, W., Lou, S., Ma, Y., Li, X., Zeng, L., Wu, Z., Zheng, J., and Guo, S.: Observational Evidence for the Involvement of Dicarboxylic Acids in Particle Nucleation, Environ. Sci. Technol. Lett., 7, 388–394, 2020.

Ferguson, E. E. and Arnold, F.: Ion chemistry of the stratosphere, Acc. Chem. Res., 14, 327–334, 1981.

Frege, C., Bianchi, F., Molteni, U., Tröstl, J., Junninen, H., Henne, S., Sipilä, M., Herrmann, E., Rossi, M. J., Kulmala, M., Hoyle, C. R., Baltensperger, U., and Dommen,

781 J.: Chemical characterization of atmospheric ions at the high altitude research station
782 Jungfraujoch (Switzerland), Atmos. Chem Phys, 17, 2613–2629, 2017.

783 Hirsikko, A., Laakso, L., Hõrrak, U., Aalto, P. P., Kerminen, V., and Kulmala, M.:
784 Annual and size dependent variation of growth rates and ion concentrations in boreal
785 forest, Boreal Env, Res, 357–369, 2005.

786 Hirsikko, A., Nieminen, T., Gagné, S., Lehtipalo, K., Manninen, H. E., Ehn, M., Hõrrak,
787 U., Kerminen, V.-M., Laakso, L., Mcmurry, P. H., Mirme, A., Mirme, S., Petäjä, T.,
788 Tammet, H., Vakkari, V., Vana, M., and Kulmala, M.: Atmospheric Chemistry and
789 Physics Atmospheric ions and nucleation: a review of observations, Atmos. Chem Phys,
790 11, 767–798, 2011.

791 Huang, W., Saathoff, H., Shen, X., Ramisetty, R., Leisner, T., and Mohr, C.: Seasonal
792 characteristics of organic aerosol chemical composition and volatility in Stuttgart,
793 Germany, Atmos. Chem. Phys., 19, 11687–11700, 2019.

794 Hyttinen, N., Kupiainen-Määttä, O., Rissanen, M. P., Muuronen, M., Ehn, M., and
795 Kurtén, T.: Modeling the Charging of Highly Oxidized Cyclohexene Ozonolysis
796 Products Using Nitrate-Based Chemical Ionization, J. Phys. Chem. A, 119, 6339–6345,
797 2015.

798 Jokinen, T., Sipilä, M., Junninen, H., Ehn, M., Lönn, G., Hakala, J., Petäjä, T., Mauldin,
799 R. L., Kulmala, M., and Worsnop, D. R.: Atmospheric sulphuric acid and neutral cluster
800 measurements using CI-APi-TOF, Atmos. Chem. Phys., 12, 4117–4125, 2012.

801 Jokinen, T., Sipilä, M., Kontkanen, J., Vakkari, V., Tisler, P., Duplissy, E.-M., Junninen,
802 H., Kangasluoma, J., Manninen, H. E., Petäjä, T., Kulmala, M., Worsnop, D. R., Kirkby,
803 J., Virkkula, A., and Kerminen, V.-M.: Ion-induced sulfuric acid–ammonia nucleation
804 drives particle formation in coastal Antarctica, Sci. Adv., 4, eaat9744, 2018.

805 Junninen, H., Ehn, M., Petäjä, T., Luosujärvi, L., Kotiaho, T., Kostiainen, R., Rohner,
806 U., Gonin, M., Fuhrer, K., Kulmala, M., and Worsnop, D. R.: A high-resolution mass
807 spectrometer to measure atmospheric ion composition, Atmos. Meas. Tech., 3, 1039–
808 1053, 2010.

809 Kawamura, K. and Bikkina, S.: A review of dicarboxylic acids and related compounds
810 in atmospheric aerosols: Molecular distributions, sources and transformation,
811 Atmospheric Res., 170, 140–160, 2016.

812 Kerminen, V.-M., Ojanen, C., Pakkanen, T., Hillamo, R., Aurela, M., and Meriläinen,
813 J.: Low-molecular-weight dicarboxylic acids in an urban and rural atmosphere, J.
814 Aerosol Sci., 31, 349–362, 2000.

815 Kirkby, J., Curtius, J., Almeida, J., Dunne, E., Duplissy, J., Ehrhart, S., Franchin, A.,
816 Gagné, S., Ickes, L., Kürten, A., Kupc, A., Metzger, A., Riccobono, F., Rondo, L.,
817 Schobesberger, S., Tsagkogeorgas, G., Wimmer, D., Amorim, A., Bianchi, F.,

Breitenlechner, M., David, A., Dommen, J., Downard, A., Ehn, M., Flagan, R. C., Haider, S., Hansel, A., Hauser, D., Jud, W., Junninen, H., Kreissl, F., Kvashin, A., Laaksonen, A., Lehtipalo, K., Lima, J., Lovejoy, E. R., Makhmutov, V., Mathot, S., Mikkilä, J., Minginette, P., Mogo, S., Nieminen, T., Onnela, A., Pereira, P., Petäjä, T., Schnitzhofer, R., Seinfeld, J. H., Sipilä, M., Stozhkov, Y., Stratmann, F., Tomé, A., Vanhanen, J., Viisanen, Y., Vrtala, A., Wagner, P. E., Walther, H., Weingartner, E., Wex, H., Winkler, P. M., Carslaw, K. S., Worsnop, D. R., Baltensperger, U., and Kulmala, M.: Role of sulphuric acid, ammonia and galactic cosmic rays in atmospheric aerosol nucleation, Nature, 476, 429–433, 2011.

Kirkby, J., Duplissy, J., Sengupta, K., Frege, C., Gordon, H., Williamson, C., Heinritzi, M., Simon, M., Yan, C., Almeida, J., Tröstl, J., Nieminen, T., Ortega, I. K., Wagner, R., Adamov, A., Amorim, A., Bernhammer, A.-K., Bianchi, F., Breitenlechner, M., Brilke, S., Chen, X., Craven, J., Dias, A., Ehrhart, S., Flagan, R. C., Franchin, A., Fuchs, C., Guida, R., Hakala, J., Hoyle, C. R., Jokinen, T., Junninen, H., Kangasluoma, J., Kim, J., Krapf, M., Kürten, A., Laaksonen, A., Lehtipalo, K., Makhmutov, V., Mathot, S., Molteni, U., Onnela, A., Peräkylä, O., Piel, F., Petäjä, T., Praplan, A. P., Pringle, K., Rap, A., Richards, N. A. D., Riipinen, I., Rissanen, M. P., Rondo, L., Sarnela, N., Schobesberger, S., Scott, C. E., Seinfeld, J. H., Sipilä, M., Steiner, G., Stozhkov, Y., Stratmann, F., Tomé, A., Virtanen, A., Vogel, A. L., Wagner, A. C., Wagner, P. E., Weingartner, E., Wimmer, D., Winkler, P. M., Ye, P., Zhang, X., Hansel, A., Dommen, J., Donahue, N. M., Worsnop, D. R., Baltensperger, U., Kulmala, M., Carslaw, K. S., and Curtius, J.: Ion-induced nucleation of pure biogenic particles, Nature, 533, 521–526, 2016.

Koenig, A. M., Magand, O., Laj, P., Andrade, M., Moreno, I., Velarde, F., Salvatierra, G., Gutierrez, R., Blacutt, L., Aliaga, D., Reichler, T., Sellegri, K., Laurent, O., Ramonet, M., and Dommergue, A.: Seasonal patterns of atmospheric mercury in tropical South America as inferred by a continuous total gaseous mercury record at Chacaltaya station (5240 m) in Bolivia, Atmos. Chem. Phys., 21, 3447–3472, 2021.

Komppula, M., Vana, M., Kerminen, V.-M., Lihavainen, H., Viisanen, Y., Horrak, U., Komsaare, K., Tamm, E., Hirsikko, A., and Laakso, L.: Size distributions of atmospheric ions in the Baltic Sea region, 2007.

Kosyakov, D. S., Ul'yanovskii, N. V., Latkin, T. B., Pokryshkin, S. A., Berzhonskis, V. R., Polyakova, O. V., and Lebedev, A. T.: Peat burning – An important source of pyridines in the earth atmosphere, Environ. Pollut., 266, 115109, 2020.

Kulmala, M., Dal Maso, M., Mäkelä, J. M., Pirjola, L., Väkevä, M., Aalto, P., Miikkulainen, P., Hämeri, K., and O'Dowd, C. D.: On the formation, growth and composition of nucleation mode particles, Tellus Ser. B Chem. Phys. Meteorol., 53, 479–490, 2001.

Kürten, A., Rondo, L., Ehrhart, S., and Curtius, J.: Calibration of a Chemical Ionization

857 Mass Spectrometer for the Measurement of Gaseous Sulfuric Acid, J. Phys. Chem. A,
858 116, 6375–6386, 2012.

859 Lee, S.-H., Reeves, J. M., Wilson, J. C., Hunton, D. E., Viggiano, A. A., Miller, T. M.,
860 Ballenthin, J. O., and Lait, L. R.: Particle Formation by Ion Nucleation in the Upper
861 Troposphere and Lower Stratosphere, Science, 301, 1886–1889, 2003.

862 Lloyd, S. P.: Least Squares Quantization in PCM, IEEE Trans. Inf. Theory, 28, 129–
863 137, 1982.

864 Manninen, H. E., Nieminen, T., Asmi, E., Gagné, S., Häkkinen, S., Lehtipalo, K., Aalto,
865 P., Vana, M., Mirme, A., Mirme, S., Hõrrak, U., Plass-Dülmer, C., Stange, G., Kiss, G.,
866 Hoffer, A., Törő, N., Moerman, M., Henzing, B., de Leeuw, G., Brinkenberg, M.,
867 Kouvarakis, G. N., Bougiatioti, A., Mihalopoulos, N., O'Dowd, C., Ceburnis, D.,
868 Arneth, A., Svenningsson, B., Swietlicki, E., Tarozzi, L., Decesari, S., Facchini, M. C.,
869 Birmili, W., Sonntag, A., Wiedensohler, A., Boulon, J., Sellegri, K., Laj, P., Gysel, M.,
870 Bukowiecki, N., Weingartner, E., Wehrle, G., Laaksonen, A., Hamed, A., Joutsensaari,
871 J., Petäjä, T., Kerminen, V.-M., and Kulmala, M.: EUCAARI ion spectrometer
872 measurements at 12 European sites – analysis of new particle formation events, Atmos.
873 Chem. Phys., 10, 7907–7927, 2010.

874 Martin, R. V., Sauvage, B., Folkins, I., Sioris, C. E., Boone, C., Bernath, P., and Ziemke,
875 J.: Space-based constraints on the production of nitric oxide by lightning, J. Geophys.
876 Res. Atmos., 112, 2007.

877 Mirme, S., Mirme, A., Minikin, A., Petzold, A., Hõrrak, U., Kerminen, V. -M., and
878 Kulmala, M.: Atmospheric sub-3 nm particles at high altitudes, Atmos. Chem. Phys.,
879 10, 437–451, https://doi.org/10.5194/acp-10-7907-2010, 2010.

880 Mirme, S. and Mirme, A.: The mathematical principles and design of the NAIS - A
881 spectrometer for the measurement of cluster ion and nanometer aerosol size
882 distributions, Atmos. Meas. Tech., 6, 1061–1071, 2013.

883 Moussallam, Y., Tamburello, G., Peters, N., Apaza, F., Schipper, C. I., Curtis, A.,
884 Aiuppa, A., Masias, P., Boichu, M., Bauduin, S., Barnie, T., Bani, P., Giudice, G., and
885 Moussallam, M.: Volcanic gas emissions and degassing dynamics at Ubinas and
886 Sabancaya volcanoes; implications for the volatile budget of the central volcanic zone,
887 J. Volcanol. Geotherm. Res., 343, 181–191, 2017.

888 Ravi Kumar, M., Prabhakar, S., Nagaveni, V., and Vairamani, M.: Estimation of gas-
889 phase acidities of a series of dicarboxylic acids by the kinetic method, Rapid Commun.
890 Mass Spectrom., 19, 1053–1057, 2005.

891 Rose, C., Sellegri, K., Velarde, F., Moreno, I., Ramonet, M., Weinhold, K., Krejci, R.,
892 Ginot, P., Andrade, M., Wiedensohler, A., Laj, P., Rose, B. C., Sellegri, K., Velarde, F.,
893 Moreno, I., Ramonet, M., Weinhold, K., Krejci, R., Ginot, P., Andrade, M.,
894 Wiedensohler, A., and Laj, P.: Frequent nucleation events at the high altitude station of

Chacaltaya (5240 m a.s.l.), Bolivia, Atmos. Environ., 102, 18–29, 2015a.

Rose, C., Sellegri, K., Asmi, E., Hervo, M., Freney, E., Colomb, A., Junninen, H., Duplissy, J., Sipilä, M., Kontkanen, J., Lehtipalo, K., and Kulmala, M.: Major contribution of neutral clusters to new particle formation at the interface between the boundary layer and the free troposphere, Atmos. Chem. Phys., 15, 3413–3428, 2015b.

Rose, C., Sellegri, K., Moreno, I., Velarde, F., Ramonet, M., Weinhold, K., Krejci, R., Andrade, M., Wiedensohler, A., Ginot, P., and Laj, P.: CCN production by new particle formation in the free troposphere, Atmos. Chem. Phys., 17, 1529–1541, 2017.

Rose, C., Zha, Q., Dada, L., Yan, C., Lehtipalo, K., Junninen, H., Mazon, S. B., Jokinen, T., Sarnela, N., Sipilä, M., Petäjä, T., Kerminen, V.-M., Bianchi, F., and Kulmala, M.: Observations of biogenic ion-induced cluster formation in the atmosphere, Sci. Adv., 4, eaar5218, 2018.

Schobesberger, S., Franchin, A., Bianchi, F., Rondo, L., Duplissy, J., Kürten, A., Ortega, I. K., Metzger, A., Schnitzhofer, R., Almeida, J., Amorim, A., Dommen, J., Dunne, E. M., Ehn, M., Gagné, S., Ickes, L., Junninen, H., Hansel, A., Kerminen, V.-M., Kirkby, J., Kupc, A., Laaksonen, A., Lehtipalo, K., Mathot, S., Onnela, A., Petäjä, T., Riccobono, F., Santos, F. D., Sipilä, M., Tomé, A., Tsagkogeorgas, G., Viisanen, Y., Wagner, P. E., Wimmer, D., Curtius, J., Donahue, N. M., Baltensperger, U., Kulmala, M., and Worsnop, D. R.: On the composition of ammonia–sulfuric-acid ion clusters during aerosol particle formation, Atmos. Chem. Phys., 15, 55–78, 2015.

Schulte, P. and Arnold, F.: Pyridinium ions and pyridine in the free troposphere, Geophys. Res. Lett., 17, 1077–1080, 1990.

Sellegri, K., Rose, C., Marinoni, A., Lupi, A., Wiedensohler, A., Andrade, M., Bonasoni, P., and Laj, P.: New Particle Formation: A Review of Ground-Based Observations at Mountain Research Stations, Atmosphere, 10, 493, 2019.

Shuman, N. S., Hunton, D. E., and Viggiano, A. A.: Ambient and Modified Atmospheric Ion Chemistry: From Top to Bottom, Chem. Rev., 115, 4542–4570, 2015.

Sims, G. K., O'Loughlin, E. J., and Crawford, R. L.: Degradation of pyridines in the environment, Crit. Rev. Environ. Control, 19, 309–340, 1989.

Skamarock, W. C., Klemp, J. B., Dudhia, J., Gill, D. O., Liu, Z., Berner, J., Wang, W., Powers, J. G., Duda, M. G., Barker, D. M., and Huang, X.-Y.: A Description of the Advanced Research WRF Model Version 4, UCAR/NCAR, 2019.

Smith, D. and Spanel, P.: Ions in the terrestrial atmosphere and in interstellar clouds, Mass Spectrom. Rev., 14, 255–278, 1995.

Venzac, H., Sellegri, K., Laj, P., Villani, P., Bonasoni, P., Marinoni, A., Cristofanelli, P., Calzolari, F., Fuzzi, S., Decesari, S., Facchini, M.-C., Vuillermoz, E., and Verza, G. P.: High frequency new particle formation in the Himalayas, Proc. Natl. Acad. Sci., 105,

15666–15671, 2008.

Wang, X.-B., Nicholas, J. B., and Wang, L.-S.: Photoelectron Spectroscopy and Theoretical Calculations of SO4- and HSO4-: Confirmation of High Electron Affinities of SO4 and HSO4, J. Phys. Chem. A, 104, 504–508, 2000.

Wiedensohler, A., Birmili, W., Nowak, A., Sonntag, A., Weinhold, K., Merkel, M., Wehner, B., Tuch, T., Pfeifer, S., Fiebig, M., Fjäraa, A. M., Asmi, E., Sellegri, K., Depuy, R., Venzac, H., Villani, P., Laj, P., Aalto, P., Ogren, J. A., Swietlicki, E., Williams, P., Roldin, P., Quincey, P., Hüglin, C., Fierz-Schmidhauser, R., Gysel, M., Weingartner, E., Riccobono, F., Santos, S., Grüning, C., Faloon, K., Beddows, D., Harrison, R., Monahan, C., Jennings, S. G., O'Dowd, C. D., Marinoni, A., Horn, H.-G., Keck, L., Jiang, J., Scheckman, J., McMurry, P. H., Deng, Z., Zhao, C. S., Moerman, M., Henzing, B., de Leeuw, G., Löschau, G., and Bastian, S.: Mobility particle size spectrometers: harmonization of technical standards and data structure to facilitate high quality long-term observations of atmospheric particle number size distributions, Atmospheric Meas. Tech., 5, 657–685, 2012.

Wiedensohler, A., Andrade, M., Weinhold, K., Müller, T., Birmili, W., Velarde, F., Moreno, I., Forno, R., Sanchez, M. F., Laj, P., Ginot, P., Whiteman, D. N., Krejci, R., Sellegri, K., and Reichler, T.: Black carbon emission and transport mechanisms to the free troposphere at the La Paz/El Alto (Bolivia) metropolitan area based on the Day of Census (2012), Atmos. Environ., 194, 158–169, 2018.

Williams, E. R.: The global electrical circuit: A review, Atmos. Res., 91, 140–152, 2009.

Wilson, C. T. R.: On a method of making visible the paths of ionising particles through a gas, Proc. R. Soc. Lond. Ser. Contain. Pap. Math. Phys. Character, 85, 285–288, 1911.

Yan, C., Dada, L., Rose, C., Jokinen, T., Nie, W., Schobesberger, S., Junninen, H., Lehtipalo, K., Sarnela, N., Makkonen, U., Garmash, O., Wang, Y., Zha, Q., Paasonen, P., Bianchi, F., Sipilä, M., Ehn, M., Petäjä, T., Kerminen, V. M., Worsnop, D. R., and Kulmala, M.: The role of H_2SO_4-NH_3 anion clusters in ion-induced aerosol nucleation mechanisms in the boreal forest, Atmos. Chem. Phys., 18, 13231–13243, 2018.

Yli-Juuti, T., Riipinen, I., Aalto, P. P., Nieminen, T., Maenhaut, W., Janssens, I. A., Claeys, M., Salma, I., Ocskay, R., Hoffer, A., Imre, K., and Kulmala, M.: Characteristics of new particle formation events and cluster ions at K-puszta, Hungary, Boreal Env Res, 14, 683–698, 2009.

Yu, F.: Ion-mediated nucleation in the atmosphere: Key controlling parameters, implications, and look-up table, J. Geophys. Res. Atmos., 115, 2010.

Zha, Q., Yan, C., Junninen, H., Riva, M., Sarnela, N., Aalto, J., Quéléver, L., Schallhart, S., Dada, L., Heikkinen, L., Peräkylä, O., Zou, J., Rose, C., Wang, Y., Mammarella, I., Katul, G., Vesala, T., Worsnop, D. R., Kulmala, M., Petäjä, T., Bianchi, F., and Ehn, M.: Vertical characterization of highly oxygenated molecules (HOMs) below and above a

970 boreal forest canopy, Atmos. Chem. Phys., 18, 17437–17450, 2018.

971 Zha, Q.: Figure data of "Measurement report: Molecular-level investigation of
972 atmospheric cluster ions at the tropical high-altitude research station Chacaltaya (5240
973 m a.s.l.) in the Bolivian Andes", https://doi.org/10.5281/zenodo.7271286, [Data set].
974 Zenodo., 2022.